On the Volume Fraction Effects of Inertial Colliding Particles in Homogeneous Isotropic Turbulence[1]

Martin Ernst[2]
Research Assistant
e-mail: martin.ernst@iw.uni-halle.de

Martin Sommerfeld
Professor
e-mail: martin.sommerfeld@iw.uni-halle.de

Mechanische Verfahrenstechnik,
Zentrum für Ingenieurwissenschaften,
Martin-Luther-Universität Halle-Wittenberg,
06099 Halle (Saale), Germany

The main objective of the present study is the investigation of volume fraction effects on the collision statistics of nonsettling inertial particles in a granular medium as well as suspended in an unsteady homogeneous isotropic turbulent flow. For this purpose, different studies with mono-disperse Lagrangian point-particles having different Stokes numbers are considered in which the volume fraction of the dispersed phase is varied between 0.001 and 0.01. The fluid behavior is computed using a three-dimensional Lattice-Boltzmann method. The carrier-fluid turbulence is maintained at Taylor microscale Reynolds number 65.26 by applying a spectral forcing scheme. The Lagrangian particle tracking is based on considering the drag force only and a deterministic model is applied for collision detection. The influence of the particle phase on the fluid flow is neglected at this stage. The particle size is maintained at a constant value for all Stokes numbers so that the ratio of particle diameter to Kolmogorov length scale is fixed at 0.58. The variation of the particle Stokes number was realized by modifying the solids density. The observed particle Reynolds and Stokes numbers are in between [1.07, 2.61] and [0.34, 9.79], respectively. In the present simulations, the fluid flow and the particle motion including particle-particle collisions are based on different temporal discretization. Hence, an adaptive time stepping scheme is introduced. The particle motion as well as the occurrence of inter-particle collisions is characterized among others by Lagrangian correlation functions, the velocity angles between colliding particles and the collision frequencies. Initially, a fluid-free particle system is simulated and compared with the principles of the kinetic theory to validate the implemented deterministic collision model. Moreover, a selection of results obtained for homogeneous isotropic turbulence is compared with in literature available DNS and LES results as well. According to the performed simulations, the collision rate of particles with large Stokes numbers strongly depends on the adopted volume fraction, whereas for particles with small Stokes numbers the influence of particle volume fraction is less pronounced. [DOI: 10.1115/1.4005681]

Keywords: solid volume fraction, Lattice-Boltzmann method, turbulence, point-particles, collision model

1 Introduction

In nature and many industrial applications, collision as well as coagulation or agglomeration processes have a significant effect on the fluid dynamic transport of particles. Clotting of blood, colloidal systems and pneumatic conveying of solid particles are only a few examples. In order to calculate the coagulation rates of particles within a specified flow configuration, the influence of different particle properties and fluid parameters on particle motion must be well understood (Ho and Sommerfeld [1]). The rate at which particles collide is the critical quantity required to model the evolution of such particle systems. In the past, a huge number of theoretical analyses on the collision rate of particles in turbulent flows have been carried out. Saffman and Turner [2] provided an approximation for the collision rate of drops in atmospheric turbulence. In their analysis, the particles were small compared to the smallest length scales of the flow, so the particles followed the turbulence completely. The resulting collision rate for mono-disperse particles is given by:

$$N = \sqrt{\frac{8\pi}{15}} n_P^2 \, d_P^3 \, \sqrt{\frac{\varepsilon}{\nu}} \tag{1}$$

where n_P is the particle number concentration, d_P is the particle diameter, ε is the dissipation rate of turbulent energy and ν is the kinematic fluid viscosity. In Eq. (1) and in the equations mentioned below, N is a collision rate per unit volume and time interval. Another limiting case was studied by Abrahamson [3]. He analyzed the motion of heavy particles suspended in high intensity turbulence neglecting external forces. According to the kinetic theory, the particle motion was completely uncorrelated concerning the fluid motion. Under assumption that all components of the particle fluctuating velocity u'_P are isotropic, the resulting collision rate for one particle class is given by Ref. [3]:

$$N = 4\sqrt{\pi} \, n_P^2 \, d_P^2 \, \sqrt{\overline{u_P'^2}} \tag{2}$$

It is well known that both limiting cases are rather rarely found in practical gas-solid systems. For this reason, Williams and Crane [4] analyzed the fluctuating relative motion of two particles in a

[1]This contribution is an extended version of the paper *FEDSM2009-78072* entitled "Direct Numerical Simulations of Colliding Particles Suspended in Homogeneous Isotropic Turbulence" which was presented at the 2009 ASME Fluids Engineering Division Summer Meeting in Vail, CO, USA and received the 2010 Robert T. Knapp Award.

[2]Corresponding author.

Contributed by the Fluids Engineering Division of ASME for publication in the JOURNAL OF FLUIDS ENGINEERING. Manuscript received April 19, 2011; final manuscript received December 20, 2011; published online March 20, 2012. Assoc. Editor: John Abraham.

turbulent gas flow and derived an expression for the collision rate of particles in turbulent flows. A more general analytical derivation based on the formulation of Williams and Crane [4] was proposed by Kruis and Kusters [5]. They took into account the effects of the particle inertia as well as the difference in densities of fluid and particles. The resulting collision rate was determined as function of the relative velocity between two equal-sized particles u_{Pij}:

$$N = \sqrt{\frac{8\pi}{3}} n_P^2 \, d_P^2 \, \sqrt{u_{Pij}^2} \tag{3}$$

In contrast to the Saffman and Turner limit, Eq. (1), and the kinetic theory, Eq. (2), where the collision timescales are based either on the turbulent dissipation rate or on the mean particle velocity fluctuations, the collision frequency is determined in this equation by the relative velocity of particle pairs. A detailed description for the calculation of the relative particle velocity for an accelerative and a shear flow can be found in Ref. [5]. Based on the derivations mentioned above, Mei and Hu [6], Alipchenkov and Zaichik [7] as well as Wang et al. [8] and Zaichik et al. [9] developed later more general statistical models for the description of the collision rate in turbulent flows.

In contrast, You et al. [10] investigated the collision rate in a vertical two-phase flow by applying particle tracking velocimetry (PTV) measurements. A detailed comparison between experiments and direct numerical simulations (DNS) of colliding inertial particles in a nearly isotropic turbulence was published by Salazar et al. [11]. The experimental setup consisted of a cubic box with single fans in the eight corners. This made it possible to sustain nearly isotropic turbulence in the center of the box [11].

Furthermore, numerical methods can be used for analyzing the influence of particle properties on collision behavior. Sundaram and Collins [12], Wang et al. [13] and Février et al. [14] examined in a deterministic frame inter-particle collisions of hard spheres in a forced isotropic turbulence applying a particle tracking method under the assumption of point-particles. Furthermore, the influence of sub-grid fluid turbulence effects on the statistics of heavy colliding particles suspended in steady homogeneous isotropic turbulence was analyzed by Fede and Simonin [15]. However, these approaches suffer from the limitations that the particle size must be smaller than the Kolmogorov length scale and the particle Reynolds number should be small to ensure Stokes flow around the particle. In the recent years, some groups overcame those limitations by applying fully-resolved simulations of finite-sized particles, e.g., Ten Cate et al. [16], Uhlmann [17], Lucci et al. [18] and Dietzel et al. [19]. In those simulations, the volume fraction of the dispersed phase was considered up to 10%. An extensive overview of the actual developments in the field of the turbulent collision of inertial particles using DNS was recently published by Wang et al. [20].

Notwithstanding of diverse investigations mentioned above, a multitude number of questions with regard to transport and collision of primary particles in turbulent flows are still unanswered. One of the major challenges is to understand the motion and hydrodynamic interaction of finite-sized particles suspended in turbulent fluid flows. At this, a subject of specific interest is the short-range hydrodynamic interaction during the approach of particles, e.g., the displacement of fluid shortly before a collision. In addition to this, the combination of other local phenomena such as the relative motion between particles, particle-particle collisions and particle segregation are of particular interest as well. For example, a specific condition is the influence of the volume fraction of the dispersed phase on the relative motion of colliding particles in turbulent flows. In literature, this effect was already partly analyzed by applying DNS [12] and large eddy simulations (LES) [21] of nonsettling spherical particles suspended in homogeneous isotropic turbulence.

Sundaram and Collins [12] compared the collision frequencies at various particle number densities by maintaining the same particle response times to ensure that the dynamic spatial arrangement and velocity distributions of particles remain identical. They observed that with increasing volume fraction the collision frequencies follow a conventional squared dependence. However, a more general implication could not be derived, since the particle Stokes number was kept constant at 1.0 [12]. Another analysis based on LES was performed by Laviéville et al. [21]. As it is to be expected, the collision frequency computed from LES was smaller than the one given by the kinetic theory and increases with increasing volume fraction with respect to the particle Stokes number. This trend was qualitatively reproduced by an analytical approximation proposed by Williams and Crane [4] (see discussion above), but the agreement is not fully satisfactory, especially for smaller Stokes numbers. Furthermore, the obtained differences between the various volume fractions were unfortunately not evaluated. Hence, the present investigations are precisely addressed to this issue.

The main objective of this contribution is to analyze the volume fraction effects of the dispersed phase on the collision statistics of nonsettling inertial particles suspended in unsteady homogeneous isotropic turbulent flow under the assumption of point-particles. The present analyses are particular focused on how an increasing volume fraction affects the relative motion of colliding particles. Moreover, this study aims to identify how the collision frequency is affected by the number concentration of particles. It would also be interesting to discover whether there are any significant differences between DNS and LES, especially when the particle diameter is smaller than the Kolmogorov length scale. For this purpose, the significance for different particle Stokes numbers is investigated and parameterized. The acquired knowledge about basic collision behavior will be necessary to improve an efficient stochastic Lagrangian collision model, proposed by Sommerfeld [22], which is principally based on the fluctuating velocity components of the real and fictitious collision partners. The present study is intended to provide the basis for aspired enhancements.

The fluid behavior is computed using a three-dimensional Lattice-Boltzmann method (LBM) including a spectral forcing scheme to generate the turbulence field. The LBM is a numerically very efficient approach for simulating laminar and turbulent flows [23]. Moreover, this method has great advantages for considering a flow with fully-resolved finite-sized particles or agglomerates which is the final objective of this study, but not part of this contribution. However, collisions between particles, either Lagrangian mass points or fully-resolved finite-sized particles, are modeled by the same deterministic collision algorithm. Hence, another goal of this study is to present a validation of the implemented collision routines using the Lagrangian approach and to compare the observed results with in literature available DNS and LES results.

The third and last objective of the present investigations is to provide a detailed dataset about collision statistics which will be used for a direct comparison of Lagrangian mass points with fully-resolved finite-sized particles. Unfortunately, at present in literature existing datasets cannot be used, since most particle properties such as volume fraction α_P or the ratio of particle diameter to Kolmogorov length scale d_P/λ_K are by definition too small for a currently practicable application of fully-resolved particles, e.g., $d_P/\lambda_K \ll 1$ and $\alpha_P \ll 0.001$. The necessary fluid domain dimensions would be too large for the resolution of the required turbulent length scales, having regard to currently available computing capacities.

The present paper is organized as follows. The simulation method including governing equations required for the performed DNS are presented in Sec. 2. In Sec. 3, first, the new implemented deterministic collision model is validated using a fluid-free particle system. Then, the turbulent carrier fluid, more precisely homogeneous isotropic turbulence, is characterized. The last subsections are dedicated to the analysis of the main results concerning particle motion as well as collision statistics. Additionally, a comparison of the obtained results with those reported in Refs. [12–21] is carried out. And finally, in Sec. 4, a conclusion of the paper as well as an outlook about further investigations is presented.

2 Method Description

In the following, the applied methods and models which were implemented in this framework are briefly described. This includes the basic equations of the Lattice-Boltzmann method, a general summary of the spectral forcing of the turbulent velocity field as well as the Lagrangian tracking of the injected primary particles and; finally, a detailed derivation of time-sequenced collision detection and the implemented algorithm.

2.1 Lattice-Boltzmann Method. The computation of the fluid flow is performed using a three-dimensional Lattice-Boltzmann method (LBM). Basically, the LBM is predicated on a highly simplified description of the micro dynamic of single fluid molecules. In doing so, the interaction between the fluid particles is not directly resolved, but modeled by the Boltzmann equation. Therefore, the discretized Boltzmann equation describes the behavior of fluids on a so-called mesoscopic level [24,25], whereas conventional models such as the Navier-Stokes equations are based on the conservation laws formulated on the macroscopic level. By applying the LBM, fictive fluid elements represented by a probability distribution function move along a lattice mesh and collide at the lattice nodes. Besides the spatial discretization realized by the numerical grid, velocity and time are discretized as well. Information is allowed to propagate to a neighboring lattice node in one of the discrete lattice directions at one time step only, followed by a collision step. The key variable of the Boltzmann equation is the discrete distribution function $f_{\sigma i}$. It represents the number of fictive fluid elements which have the velocity $\boldsymbol{\xi}_{\sigma i}$ at the location $\mathbf{x}$ and the time t. Fluid density and momentum can be derived as moments of the discrete distribution function:

$$\rho(\mathbf{x},\ t) = \sum_{\sigma}\sum_{i} f_{\sigma i}(\mathbf{x},\ t) \tag{4}$$

$$\rho(\mathbf{x},\ t)\ \mathbf{u}(\mathbf{x},\ t) = \sum_{\sigma}\sum_{i} \boldsymbol{\xi}_{\sigma i} f_{\sigma i}(\mathbf{x},\ t) \tag{5}$$

The Lattice-Boltzmann equation, Eq. (6), characterizes the temporal development of $f_{\sigma i}$. It is solved with the help of the single relaxation time collision operator approximated by the Bhatnagar-Gross-Krook (BGK) approach [26]:

$$f_{\sigma i}(\mathbf{x} + \boldsymbol{\xi}_{\sigma i}\Delta t,\ t + \Delta t) - f_{\sigma i}(\mathbf{x},\ t) = -\frac{\Delta t}{\tau}\left(f_{\sigma i}(\mathbf{x},\ t) - f^{(0)}_{\sigma i}(\mathbf{x},\ t)\right) + \Delta t\, F_{ext,i} \tag{6}$$

where $f^{(0)}_{\sigma i}$ is the discrete equilibrium distribution function, Δt the length of one time step, $\Delta x = \xi_{\sigma i}\,\Delta t$ the width of the spatial discretization and τ the relaxation time. The forcing term $F_{ext,i}$ is used to introduce an external vector-valued force $\mathbf{F}$ into the Lattice-Boltzmann equation. In this study, the forcing term of Guo et al. [27] is applied:

$$F_{ext,i} = \left(1 - \frac{1}{2\tau}\right)\omega_{\sigma i}\left(\frac{\boldsymbol{\xi}_{\sigma i} - \mathbf{u}}{c_s^2} + \frac{\boldsymbol{\xi}_{\sigma i} - \mathbf{u}}{c_s^4}\boldsymbol{\xi}_{\sigma i}\right)\cdot\mathbf{F} \tag{7}$$

Here, parameter c_s is the speed of sound and $\mathbf{u}$ is the fluid velocity. The number of available discrete velocity directions σi that connect the lattice nodes with each other depends on the applied model. This study uses the D3Q19 model shown in Fig. 1 which applies to a three-dimensional grid and provides 19 propagation directions. These directions can be distinguished in six vertical and horizontal velocity vectors ($\sigma = 1$), twelve diagonal velocity vectors ($\sigma = 2$) and one direction for zero velocity ($\sigma = 0$). During the propagation step, information is transported along these lattice directions—left side of Eq. (6)—followed by the collision step—right side of Eq. (6). The discretized equilibrium distribution $f^{(0)}_{\sigma i}$ and the appropriate weighting factors for the D3Q19 model $\omega_{\sigma i}$ are given below:

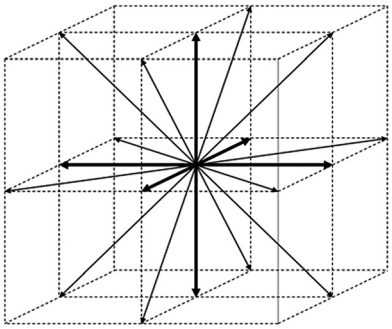

Fig. 1 Velocity direction vectors of the D3Q19 model

$$f^{(0)}_{\sigma i}(\mathbf{x},t) = \omega_{\sigma i}\,\rho\left(1 + \frac{3\,\boldsymbol{\xi}_{\sigma i}\,\mathbf{u}}{c^2} + \frac{9\,(\boldsymbol{\xi}_{\sigma i}\,\mathbf{u})^2}{2c^4} - \frac{3\mathbf{u}^2}{2c^2}\right) \tag{8}$$

$$\omega_{\sigma i} = \begin{cases} 1/3\ ; & \sigma = 0,\ i = 1 \\ 1/18\ ; & \sigma = 1,\ \ i = 1...6 \\ 1/36\ ; & \sigma = 2,\ i = 1...12 \end{cases} \tag{9}$$

Furthermore, a grid constant c can be defined as a ratio of spatial and temporal discretization which is related to the speed of sound c_s. The local pressure can be derived from the local density and the speed of sound using Eqs. (10) and (11):

$$c = \frac{\Delta x}{\Delta t} = \sqrt{3}\,c_s \tag{10}$$

$$p(\mathbf{x},\ t) = c_s^2\,\rho(\mathbf{x},\ t) = \frac{1}{3}\frac{\Delta x^2}{\Delta t^2}\,\rho(\mathbf{x},\ t) \tag{11}$$

The relation between the dynamic viscosity of the Lattice-Boltzmann scheme and the relaxation parameter τ can be described in the following way:

$$\eta = \frac{1}{6}\rho\,c^2\,(2\tau - \Delta t) \tag{12}$$

A more detailed method description as well as examples of end use fields of the applied LBM can be found in Dietzel et al. [19] and Dietzel and Sommerfeld [28].

2.2 Turbulence Forcing. The spectral forcing scheme of Eswaran and Pope [29] is used to generate isotropic turbulence. Turbulence is realized by generating a force in spectral space and introducing it as a change of velocity in the flow field. As a result, motion is created at large length scales. This is the basis for the development of motion at small length scales in form of an energy cascade which dissipates over time. For this purpose, the complete three-dimensional velocity field is transformed during each time step into spectral space by the following Fourier transformation:

$$\tilde{\mathbf{u}}(\mathbf{k},t) = \frac{1}{N_{Cells}}\sum_{l_1}\sum_{l_2}\sum_{l_3}\mathbf{u}(\mathbf{x},t)e^{(-i\mathbf{k}\mathbf{x})} \tag{13}$$

where N_{Cells} is the total number of cells. The parameter $\tilde{\mathbf{u}}(\mathbf{k},t)$ indicates the corresponding Fourier coefficient of the fluid velocity at the wave number $\mathbf{k}$ and the time t. In the applied scheme,

the forcing is performed by adding a forcing acceleration $\tilde{\mathbf{a}}_\mathbf{F}$ to the given fluid acceleration $\tilde{\mathbf{a}}$ during a fluid time step [29]:

$$\frac{d\,\tilde{\mathbf{u}}(\mathbf{k},t)}{dt} = \tilde{\mathbf{a}}(\mathbf{k},t) + \tilde{\mathbf{a}}_\mathbf{F}(\mathbf{k},t) \tag{14}$$

Since large eddies should be created, the forcing acceleration is only applied in a low wave number band. Hence, the largest forced wave number $k_{F,max}$ is equal to or less than two. For each forced wave number, the implemented procedure combines six independent Uhlenbeck-Ornstein stochastic processes [30]:

$$\Re,\Im: \quad \tilde{\mathbf{a}}_\mathbf{F}(\mathbf{k},t+\Delta t) = \left(1-\frac{\Delta t}{T_F}\right)\tilde{\mathbf{a}}_\mathbf{F}(\mathbf{k},t) + \Gamma\, Z_F \sqrt{\frac{2\,\sigma_F^2\,\Delta t}{T_F}} \tag{15}$$

This process is characterized by the correlation timescale T_F, the forcing amplitude σ_F and a Gaussian random number Γ with a mean of zero and variance of one. The forcing is limited to the range of wave numbers by a forcing cut-off function Z_F, proposed by Overholt and Pope [31]:

$$Z_F = \tanh\left(\frac{k_{F,\max}-k}{\zeta\, k_{F,\max}}\right) H\left(k_{F,\max}-k\right) \tag{16}$$

The abruptness of the cut-off was determined experimentally and is defined as $\zeta = 0.2$ [31]. After the forcing within the given time step is completed, the three-dimensional velocity field is transformed back into physical space via an inverse Fourier transformation (in analogy to Eq. (13)). Under application of these equations and fully periodic boundary conditions, the homogeneous isotropic turbulence field is generated over the entire computational domain.

2.3 Lagrangian Particle Tracking. The transport of monodisperse spherical particles is simulated by the Lagrangian approach which considers a discrete particle traveling in a continuous fluid medium. Since periodic boundary conditions are applied, particles leaving the computational domain are reinjected on the opposite side with the same velocity. The change of the particle location and the linear components of the particle velocity are calculated by solving a set of ordinary differential equations along the particle trajectory [32]:

$$\frac{d\mathbf{x_P}}{dt_P} = \mathbf{u_P} \tag{17}$$

$$m_P \frac{d\mathbf{u_P}}{dt_P} = \sum \mathbf{F_i} \tag{18}$$

Here, $\mathbf{x_P}$ is the particle position vector, $\mathbf{u_P}$ is the particle linear velocity vector, m_P is the particle mass, Δt_P the Lagrangian particle time step and $\mathbf{F_i}$ represents the different relevant forces acting on the particle. These equations, which are solved simultaneously for all particles in the computational domain, determine the momentum transfer from the fluid phase to the particles and vice versa.

Since the particles are restricted to densities much larger than the fluid and to diameters explicitly larger than the molecular free path of the fluid, a random force due to Brownian motion is neglected. Moreover, by applying particle densities much larger than the fluid density, the particle motion may be dominated by the drag force $\mathbf{F_d}$. This assumption is underlined through the investigations by Hjelmfelt and Mockros [33], in which the influence of different forces within the equation of motion was successive analyzed. For this reason, $\mathbf{F_d}$ is considered in the equation of motion for the particles only and is given by:

$$\mathbf{F_d} = \frac{m_P\,(\mathbf{u}-\mathbf{u_P})}{\tau_P} \tag{19}$$

where the particle response time τ_P is defined as:

$$\tau_P = \frac{\rho_P\, d_P^2}{18\,\eta}\,\frac{24}{c_d\, Re_P} \tag{20}$$

with the particle Reynolds number:

$$Re_P = \frac{\rho\, d_P\, |\mathbf{u}-\mathbf{u_P}|}{\eta} \tag{21}$$

The fluid velocity $\mathbf{u}$ is extracted at the position of the particles (locally undisturbed by the particles), whereby the vector-valued components are determined by a trilinear interpolation method using the eight nearest fluid nodes neighbored to the given particle position. Nevertheless, this approach could lead to deviations, since the applied interpolation procedure reconstructs the fluid velocities of a complex eddy structure only to a certain degree.

For the drag coefficient c_d the following correlation for a single sphere, proposed by Schiller and Naumann [34], is used:

$$\begin{aligned} c_d &= \frac{24}{Re_P}\left(1+0.15\,Re_P^{0.687}\right), && Re_P < 1000 \\ c_d &= 0.44\,, && Re_P \geq 1000 \end{aligned} \tag{22}$$

However, the drag coefficient of a particle in a two-phase flow is partly affected by the existence and movement of neighboring particles. In addition, the presence of fluid shortly before a collision causes a lubrication force. Those short-range phenomena may partly influence the interaction between particles. But in order to realize a comparison with previously published DNS results such as [12,15], the modification of turbulence by the particles and the hydrodynamic interaction between particles is not considered. Nevertheless, it should keep in mind that these simplifications may have certain effects on the observed collision statistics.

In order to calculate the particle motion, the Eqs. (17) and (18) were integrated over Δt_P. The integration was performed using an analytical approach presented by Sommerfeld [35]. The relevant time step is calculated in an adaptive way and is chosen by the global minima of the time required to cross the half length of a computational cell, the particle response time and the time to cross a turbulent eddy. At this, the time between two particle-particle collisions plays only a subordinate role, since the deterministic resolution of inter-particle collisions is realized by a time-sequenced collision algorithm. However, to avoid the occurrences of interpenetrations, the resulting maximum time step is in turn limited through an additional condition which is defined as will be described below (Eq. (25)).

Fluid flow and particle motion are calculated with different temporal discretization. Generally, the time step Δt for the LBM is larger than the time step restrictions for the particle tracking. After the simulation of the flow field all particles are tracked simultaneously with the identical time step Δt_P until the new time level is reached. Then the fluid flow is recalculated until the next time level. Hence, during the Lagrangian tracking the particles view a frozen flow field.

2.4 Deterministic Collision Algorithm. In a particulate turbulent flow, the determination of particle trajectories and particle collisions depends both on the particle-particle interactions and on the temporal and spatial varying turbulence. Because the particles are affected by the time-varying flow field, inter-particle collisions cannot be projected forward in time indefinitely. In the framework of the presented study, the detection and modeling of particle-particle collisions is computed using a deterministic collision model proposed by Sundaram and Collins [36]. This model assumes that the collisions are binary and quasi-instantaneous. Furthermore, the inelastic contact between two hard spheres occurs in a single point. In order to determine whether a collision

occurs, a time-sequenced collision detection and accomplishment algorithm is applied. A program flow chart of the implemented method is shown in Fig. 2.

At first, all particles are tracked to the end of the present Lagrangian particle time step. Inter-particle collisions have occurred, if particles overlap after the actual time interval. In the case of a collision, the distance between the centers is equal to or less than the half sum of the two particle diameters. This condition can be written as:

$$\left| \mathbf{x_{Pij}}(t+\Delta t) \right| \leq 0.5 \left(d_{Pi} + d_{Pj}\right) \tag{23}$$

The determination of all existing collision pairs is realized under application of the cell-index method [37]. The potential collision partners of a given particle are found among the other particles in the cell plus the particles in all 26 neighboring cells. The list of particles in each cell is set up and updated using linked lists. Assuming that the particles move at constant velocities during the particle time step, the collision time for each overlapping pair $\Delta t_{ij,c}$ is calculated by solving the following quadratic equation:

$$\left| \mathbf{x_{Pij}}\,(t+\Delta t) \;+ \mathbf{u_{Pij}}\,(t+\Delta t)\,\Delta t_{ij,c} \right| = 0.5\,\left(d_{Pi} + d_{Pj}\right) \tag{24}$$

Equation (24) suffers from the limitation that it will not detect a particle-particle collision, if complete interpenetration occurs during the given particle time step. To minimize the occurrences of interpenetrations the particle time step should satisfy the next condition [36]:

$$\frac{u_{P,max}\,\Delta t_P}{d_P} \ll 1.0 \tag{25}$$

Subsequently, the determined collision times (i.e., the time between the beginning of the actual time step and the time of particle collisions) are sorted in descending order. In the time-sequenced implementation, the first overlapping pair is moved backward in time to the position of collision. The determination of the post-collision velocities $\mathbf{u^*_{Pi}}$ and $\mathbf{u^*_{Pj}}$ of the collision couple is based on the laws of impact provided by Tanaka and Tsuji [38]. The new linear velocity components of both particles $\mathbf{u^*_P}$ are calculated in terms of the velocity components before the collision $\mathbf{u_P}$:

$$\mathbf{u^*_{Pi}} = \mathbf{u_{Pi}} + \frac{\mathbf{J}}{m_{Pi}} \tag{26}$$

$$\mathbf{u^*_{Pj}} = \mathbf{u_{Pj}} - \frac{\mathbf{J}}{m_{Pj}} \tag{27}$$

In the above equation, m_{Pi} and m_{Pj} are the masses of each particle and $\mathbf{J}$ is the vector of the momentum. As presented in Fig. 3, the momentum vector can be divided into normal J_n and tangential J_t components:

$$\mathbf{J} = J_n\,\mathbf{e_n} + J_t\,\mathbf{e_t} \tag{28}$$

where $\mathbf{e_n}$ is the normal and $\mathbf{e_t}$ is the tangential unit vector. The normal unit vector directed from particle i to j is given by:

$$\mathbf{e_n} = \frac{\mathbf{x_{Pj}} - \mathbf{x_{Pi}}}{\left|\mathbf{x_{Pj}} - \mathbf{x_{Pi}}\right|} \tag{29}$$

Using the relative velocity between both particles $\mathbf{u_{Pij}}$, the tangential slip velocity of the particle j to particle i at the point of contact $\mathbf{u_{Pij,t}}$ and the tangential unit vector $\mathbf{e_t}$ can be written as:

$$\mathbf{u_{Pij,t}} = \mathbf{u_{Pij}} - \left(\mathbf{e_n} \cdot \mathbf{u_{Pij}}\right) \mathbf{e_n} \tag{30}$$

$$\mathbf{e_t} = \frac{\mathbf{u_{Pij,t}}}{\left|\mathbf{u_{Pij,t}}\right|} \tag{31}$$

A relationship between the normal relative velocity of the particles before and after the impact is created by introducing the normal restitution coefficient e:

$$e = -\frac{\mathbf{e_n} \cdot \mathbf{u^*_{Pij}}}{\mathbf{e_n} \cdot \mathbf{u_{Pij}}} \tag{32}$$

The following equation describes the skew of an impact. During a head-on collision the skew parameter ψ is zero while with ψ greater than zero a skew collision occurs.

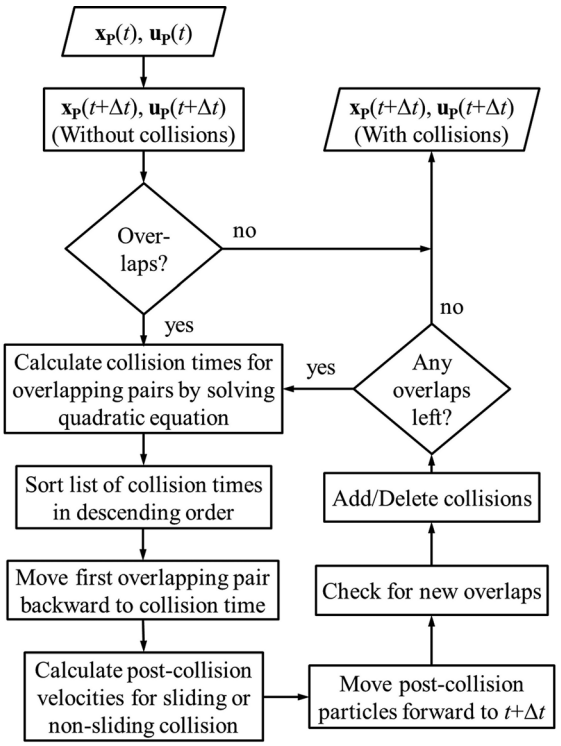

Fig. 2 Program flow chart for the deterministic collision model (in analogy to Ref. [36]).

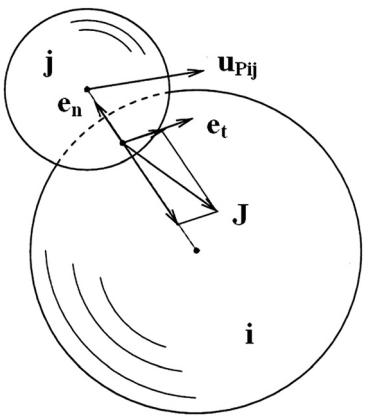

Fig. 3 Pictorial representation of two colliding particles [38]

$$\psi = \frac{\left|\mathbf{u}_{\mathbf{Pij,t}}\right|}{\mathbf{e_n} \cdot \mathbf{u_{Pij}}} \tag{33}$$

In case of a nonsliding impact, the tangential restitution coefficient becomes zero and the dynamic coefficient of friction μ_d must be replaced by the static friction coefficient μ_s. Under application of this relationship, the limiting skew parameter ψ_0 can be defined as:

$$\psi_0 = 3.5\ \mu_s\ (1+e) \tag{34}$$

For a nonsliding collision, the skew parameter is equal to or less than the limiting skew parameter. In this case, the new linear velocities of both particles $\mathbf{u}_\mathbf{P}^*$ can be calculated by:

$$\mathbf{u}_{\mathbf{Pi}}^* = \mathbf{u_{Pi}} - \frac{m_{Peff}}{m_{Pi}} \left[(1+e)\ \left(\mathbf{e_n} \cdot \mathbf{u_{Pij}}\right)\ \mathbf{e_n} + \frac{2}{7}\ u_{Pij,t}\ \mathbf{e_t} \right] \tag{35}$$

$$\mathbf{u}_{\mathbf{Pj}}^* = \mathbf{u_{Pj}} + \frac{m_{Peff}}{m_{Pj}} \left[(1+e)\ \left(\mathbf{e_n} \cdot \mathbf{u_{Pij}}\right)\ \mathbf{e_n} + \frac{2}{7}\ u_{Pij,t}\ \mathbf{e_t} \right] \tag{36}$$

where the effective particle mass m_{Peff} is defined as:

$$m_{Peff} = \frac{m_{Pi}\ m_{Pj}}{m_{Pi} + m_{Pj}} \tag{37}$$

If the skew parameter is greater than the limiting one, a sliding collision occurs. The new components of the particle velocities depend in this case on the dynamic coefficient of friction, see Eqs. (38) and (39). A detailed derivation of the present collision operators can be found in the Ph.D. thesis of Decker [39].

$$\mathbf{u}_{\mathbf{Pi}}^* = \mathbf{u_{Pi}} - (1+e)\ \frac{m_{Peff}}{m_{Pi}}\ \left(\mathbf{e_n} \cdot \mathbf{u_{Pij}}\right)\ \left(\mathbf{e_n} - \mu_d\ \mathbf{e_t}\right) \tag{38}$$

$$\mathbf{u}_{\mathbf{Pj}}^* = \mathbf{u_{Pj}} + (1+e)\ \frac{m_{Peff}}{m_{Pj}}\ \left(\mathbf{e_n} \cdot \mathbf{u_{Pij}}\right)\ \left(\mathbf{e_n} - \mu_d\ \mathbf{e_t}\right) \tag{39}$$

After the executed inelastic collision, both particles are again moved forward to complete the actual particle tracking time step. New overlaps may be added to the list of colliding particles, i.e., in the case of multiple particle collisions within one tracking time step, while processed or nonexistent ones are deleted. These collision computations are carried out until no overlaps are left.

3 Discussion of Results

In this section, the main results of the performed direct numerical simulations are discussed. After a short validation of the implemented deterministic collision model using a fluid-free particle system (i.e., granular medium), the characterization of the turbulent fluid phase is introduced. Subsequently, the motion of colliding particles, which are suspended in unsteady homogeneous isotropic turbulence, is analyzed among others through the obtained collision frequencies as a function of various solid volume fractions.

As already mentioned, the used method basically consists of a spectral turbulence forcing scheme based on LBM and a Lagrangian point-mass particle tracking including a drag-law model and a deterministic description of inter-particle collisions. This is a standard approach and well established in literature. Therefore, the present results may allow a review as well as a possible reassessment of previously published results with respect to the observed influence of the volume fraction.

3.1 Fluid-Free Particle System. In accordance with Sundaram and Collins [12], the previously described deterministic collision model was validated in a fluid-free particle system. The computational domain is a cubic box with fully periodic boundaries. At the beginning of these calculations, all particles are initialized with random nonoverlapping initial positions. Based on the kinetic theory, the initial velocities of the injected particles correspond to a Maxwellian velocity distribution [12]. The collision between two hard spheres is adopted as fully inelastic. Hence, the coefficients of restitution, static friction and dynamic friction are set to 1.0, 0.0 and 0.0. Since no fluid forces are considered, the particle motion is solely affected by inter-particle collisions. For this reason, the total momentum of two colliding particles as well as the total kinetic energy summed up over all particles in the system should be preserved.

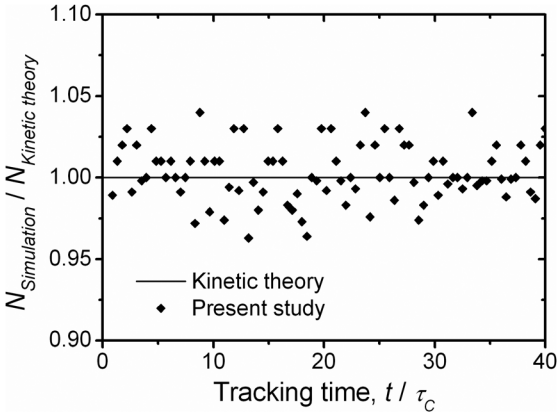

Fig. 4 Fluctuation of collision rates *N* observed in a fluid-free particle system as a function of the nondimensional tracking time (closed symbols). The solid line indicates the theoretical reference value based on the kinetic theory, cf. Eq. (2).

Figure 4 presents the time-dependent developing of the collision rate observed from the simulation related to the collision rate obtained from the principles of the kinetic theory. According to the kinetic theory, the relative motion of the particles is completely uncorrelated to each other. This behavior was analyzed by Abrahamson [3] and is given by Eq. (2). As illustrated in Fig. 4, the ratio of the observed collision rate to the theoretical collision rate fluctuates around the given analytical solution of 1.0. The maximum difference is about 5.0%. This small deviation may be caused by variations in the spatial distribution of the particles such as preferential concentration.

For verifying the energy conservation of the present fluid-free system, the probability density functions of the particle velocity modulus at the beginning of a simulation as well as the velocity modulus of colliding particles measured during a simulation are compared in Fig. 5. In this case, the velocity distribution of the initialized particles corresponds to the kinetic theory. As a result, the shapes of both distributions show an adequate agreement. For this reason, the energy content of the system is preserved when inter-particle collisions take place. The present comparison of numerical and theoretical results (see Figs. 4 and 5) indicates the correctness of the implemented collision routines.

3.2 Homogeneous Isotropic Turbulence. In the present analysis, Lagrangian particles are tracked in a homogeneous isotropic turbulent flow. The particles are suspended in a fluid with density $\rho_F = 1.17$ kg/m^3 and kinematic viscosity $\nu = 1.47 \times 10^{-5}$ m^2/s. The computational domain is a cubic box of 64^3 cells with fully periodic boundaries. This is a standard configuration in turbulence research and allows comparison with literature, e.g., Sundaram and Collins [12], Fede and Simonin [15], Laviéville et al. [21] and Sommerfeld [22]. To generate a statistically well founded initial turbulent flow field, the particle-free fluid flow was forced for six eddy turnover times. Typical turbulence characteristics resulting from this simulation are summarized in Table 1, similar to the model studies in Refs. [12,15], which are additionally listed in Table 1 for easy comparison.

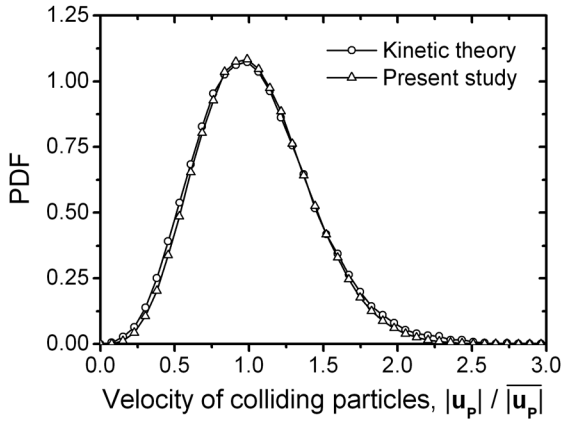

Fig. 5 Comparison of the probability density functions of the velocity modulus between colliding particles with theoretical results from the kinetic theory. The kinetic theory corresponds to the velocity distribution of the injected particles.

Turbulent kinetic energy k_F and dissipation rate ε of the turbulent fluid flow are evaluated from the three-dimensional energy spectrum $E(k)$, which is computed using the Fourier-transformed turbulent velocity field:

$$k_F = \int_0^{k_{\max}} E(k)\, dk \tag{40}$$

$$\varepsilon = 2\nu \int_0^{k_{\max}} k^2\, E(k)\, dk \tag{41}$$

In homogeneous isotropic turbulence, the integral length scale λ_{Int} can be computed also from the three-dimensional energy spectrum as follows:

$$\lambda_{Int} = \frac{3\pi}{4\,k_F} \int_0^{k_{\max}} \frac{E(k)}{k}\, dk \tag{42}$$

The root mean square (r.m.s.) of the turbulent fluid velocity fluctuations u' and the related integral timescale τ_{Int} are given by:

$$u' = \left(\frac{2k_F}{3}\right)^{1/2} \tag{43}$$

$$\tau_{Int} = \frac{\lambda_{Int}}{u'} \tag{44}$$

The Taylor microscale λ_T is obtained by the following equation, where $E_x(k)$ is the transverse one-dimensional energy spectrum [15]:

$$\lambda_T = \frac{2u'}{\int_0^{k_{\max}} k^2\, E_x(k)\, dk} \tag{45}$$

The corresponding Taylor Reynolds number Re_T is defined as:

$$Re_T = \frac{u'\,\lambda_T}{\nu} \tag{46}$$

Finally, the Kolmogorov length and time scales, λ_K and τ_K, are given by:

$$\lambda_K = \left(\frac{\nu^3}{\varepsilon}\right)^{1/4} \tag{47}$$

$$\tau_K = \left(\frac{\nu}{\varepsilon}\right)^{1/2} \tag{48}$$

In a general way, the present Taylor Reynolds number may be slightly too high with respect to the realized computational grid which was a compromise between spatial resolution and computational time. It is well established that higher resolutions ensure a better separation of the turbulent length scales and a more pronounced inertial range. However, this study is focused on particles which are smaller than the Kolmogorov length scale. Here, the transport of particles is mainly controlled by the fluid phenomena based on the smallest scales. For this reason, a detailed resolution of larger turbulent length scales is not mandatory. Nevertheless, the dynamics in the dissipation range are as well represented at the applied resolution as in higher ones. Figure 6 shows an exemplary turbulent flow field generated by the spectral method. The corresponding three-dimensional energy and dissipation spectra as well as the universal Kolmogorov spectrum are shown in Figs. 7 and 8.

Due to the still low Taylor Reynolds number reached in the simulation, an exact inertial sub-range cannot exist. This fact is pointed out by the Kolmogorov spectrum (slope −5/3) which represents the theoretical shape of the inertial sub-range at the same Re_T (see Fig. 7). However, a limitation of the Kolmogorov hypotheses is that they apply only to high-Reynolds-number flows [40]. But an exact criterion for sufficiently high Reynolds number is not provided. Nevertheless, for a good resolution of the smallest turbulent length scales, the below-mentioned criteria should be satisfied.

Table 1 Turbulence characteristics computed from the present DNS based on LBM and, besides, turbulent fluid flow statistics from other DNS, published by Sundaram and Collins (S & C) [12] and Fede and Simonin (F & S) [15].

Parameter	Symbol	LBM	S & C	F & S
Number of cells	N_{Cells}	64^3	64^3	128^3
Length of box (m)	L_{Box}	3.84×10^{-2}	6.28×10	1.28×10^{-1}
Kinematic fluid viscosity (m^2/s)	ν	1.47×10^{-5}	1.26×10^{-2}	1.47×10^{-5}
Turbulent kinetic energy (m^2/s^2)	k_F	6.15×10^{-2}	1.10×10	6.56×10^{-3}
r.m.s. fluid velocity (m/s)	u'	2.03×10^{-1}	8.55×10^{-1}	6.61×10^{-2}
Dissipation rate (m^2/s^3)	ε	2.18×10^{-1}	2.15×10^{-1}	1.63×10^{-2}
Integral length scale	λ_{Int}/L_{Box}	0.24	0.26	0.11
Integral timescale	τ_{Int}/τ_K	5.59	7.96	7.15
Taylor microscale	λ_T/λ_{Int}	0.51	0.49	0.56
Kolmogorov length scale	λ_K/λ_{Int}	3.74×10^{-2}	3.35×10^{-2}	4.80×10^{-2}
Kolmogorov timescale (s)	τ_K	8.21×10^{-3}	2.42×10^{-1}	2.88×10^{-2}
Kolmogorov velocity	u_K/u'	0.21	0.27	0.36
Max. possible wave number	$k_{max}\,\lambda_K$	1.82	1.77	2.01
Spatial discretization	$\Delta x/\lambda_K$	1.72	1.79	1.47
Taylor Reynolds number	Re_T	65.26	54.20	34.10

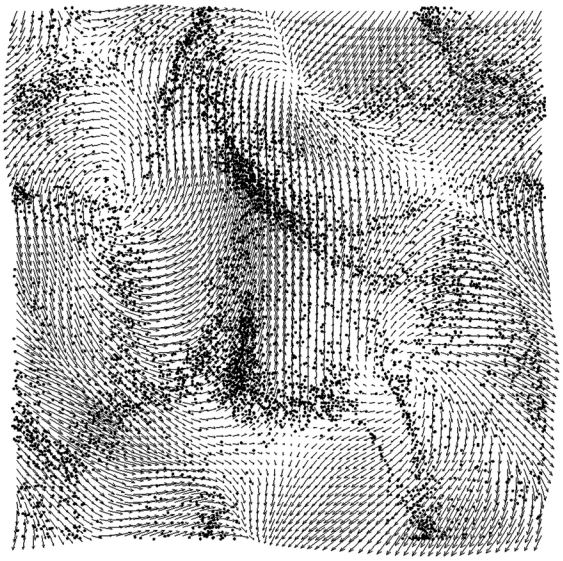

Fig. 6 Fluid velocity field (vector plot) and particle field distribution (spheres, $St = 2.57$, $\alpha_P = 0.01$) for a single plane in the computational domain.

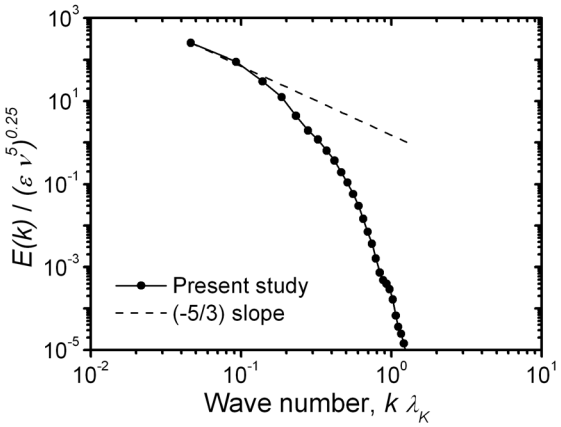

Fig. 7 Three-dimensional energy spectrum of the turbulent flow field (solid line with symbols: $Re_T = 65.26$) and Kolmogorov spectrum (dashed line: universal Kolmogorov constant $C = 1.5$) as a function of the nondimensional wave number.

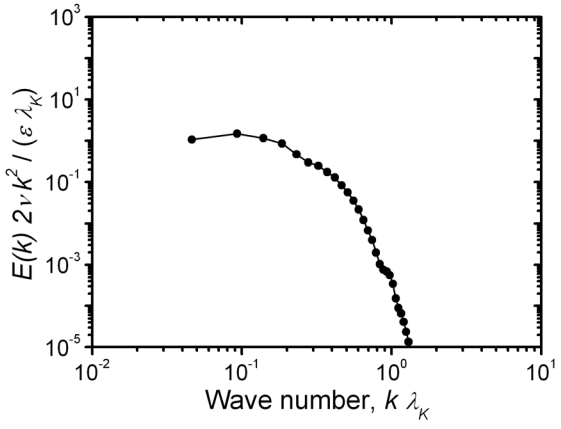

Fig. 8 Viscous dissipation spectrum computed from the present DNS ($Re_T = 65.26$) and plotted against the nondimensional wave number.

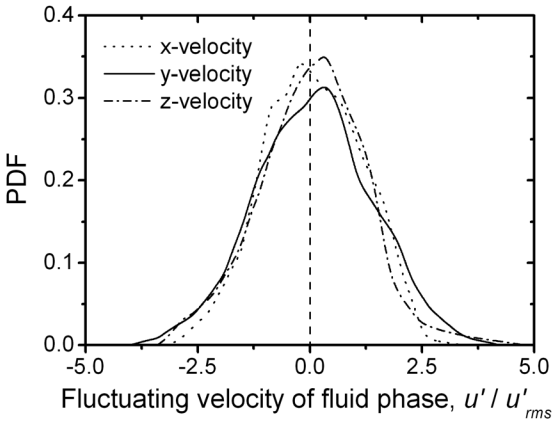

Fig. 9 Probability density functions of the fluid velocity fluctuations for the three velocity components averaged over a single eddy turnover time.

It is widely accepted that the product of maximum possible wave number and Kolmogorov length scale $k_{\max} \lambda_K$ should be greater than unity. Moreover, the ratio of spatial discretization to the Kolmogorov length scale $\Delta x/\lambda_K$ should be equal to or less than two [41]. Another indicator for an adequate resolution of the smallest length scales is the maximum appearing in the dissipation spectrum $k_{\text{Peak}} \lambda_K$ (see Fig. 8). The dissipative scales are well resolved when the maximum of the dissipation spectrum is well before $k \lambda_K \approx 1$ [29]. In the present DNS, all three criteria are fulfilled, namely $\Delta x/\lambda_K = 1.72$, $k_{\max} \lambda_K = 1.82$ and $k_{\text{Peak}} \lambda_K = 0.09$.

Even though the in Table 1 specified Taylor Reynolds numbers are somewhat different (i.e., $Re_T = 65.26$ (present study), $Re_T = 54.20$ [12] and $Re_T = 34.10$ [15]), the computed Kolmogorov length scales are more comparable (see Table 1). For this reason, the in Refs. [12,15] published particle statistics are used for comparison with results obtained from the present study. In addition to that, the obtained Taylor Reynolds number may be suitable for a comparison with particle-resolved simulations of turbulent flows laden with solid particles, where Re_T was maintained at 60.98 [16]. Figure 9 illustrates the probability density functions (PDF) of the fluid velocity fluctuations. All three curves show the typical shape of a normal distribution with a mean of zero. By reason of the nearly identical distributions, the generated turbulence can be identified as isotropic. Isotropy is reached, since the turbulence was generated with random numbers, which suffice a normal distribution with a mean of zero.

3.3 Properties of the Dispersed Phase. At the beginning of a simulation, all particles are introduced with a random nonoverlapping position inside the entire computational domain. The initial particle velocity equals the local instantaneous fluid velocity. In order to have particle response times which are in the order of the Kolmogorov timescale, the ratio of particle material density to fluid density was varied between 21 and 684 (see Table 2).

The particle diameter d_P is smaller than the Kolmogorov length scale λ_K and selected as $d_P/\lambda_K = 0.58$, having regard to spatial resolution versus currently available computing capacities. In addition, this ratio is oriented to previous DNS based on point-particle approaches as well, where the ratio d_P/λ_K was set to 0.36 [12] and 0.92 [15], respectively. It is recalled that the used particle diameter may be slightly too large with respect to the smallest scales of the present turbulent carrier fluid, since the point-particle approach is valid beyond doubt for $d_P/\lambda_K \ll 1$, cf., Maxey and Riley [42]. The constriction of the applied ratio d_P/λ_K should be kept in mind for the analysis of the obtained results. Nevertheless, the particle motion is solely affected by turbulence and inter-particle collisions, since the drag force is considered only.

Table 2 Nondimensional particle properties and collision statistics from the DNS averaged over ten eddy turnover times (Case A-F: $\alpha_P = 0.001$, Case G-M: $\alpha_P = 0.005$, and Case N-S: $\alpha_P = 0.01$).

Case	ρ_P/ρ_F	m_P/m_F	Re_P	τ_P/τ_K	$\tau_{L,P}/\tau_K$	$\tau_{L,F}/\tau_K$	τ_C/τ_K	τ_P/τ_C
A	21.37	0.02	1.07	0.34	2.25	1.55	91.73	3.71×10^{-3}
B	42.74	0.04	1.29	0.67	2.62	1.52	79.55	8.40×10^{-3}
C	85.47	0.09	1.51	1.31	3.24	1.53	43.45	3.02×10^{-2}
D	170.94	0.17	1.80	2.57	4.08	1.45	29.82	8.62×10^{-2}
E	341.88	0.34	2.16	5.02	5.51	1.47	27.01	1.86×10^{-1}
F	683.76	0.68	2.56	9.79	7.91	1.46	26.78	3.66×10^{-1}
G	21.37	0.11	1.06	0.34	2.29	1.59	31.89	1.07×10^{-2}
H	42.74	0.21	1.29	0.67	2.65	1.54	16.50	4.05×10^{-2}
I	85.47	0.43	1.51	1.31	3.19	1.51	7.47	1.76×10^{-1}
K	170.94	0.85	1.79	2.57	3.84	1.43	5.53	4.65×10^{-1}
L	341.88	1.71	2.16	5.02	4.97	1.45	5.11	9.83×10^{-1}
M	683.76	3.42	2.61	9.76	6.15	1.48	5.03	1.94×10
N	21.37	0.21	1.08	0.34	2.15	1.47	15.33	2.22×10^{-2}
O	42.74	0.43	1.27	0.67	2.61	1.52	8.17	8.18×10^{-2}
P	85.47	0.85	1.51	1.31	3.07	1.45	3.79	3.46×10^{-1}
Q	170.94	1.71	1.80	2.57	3.66	1.41	2.48	1.04×10
R	341.88	3.42	2.15	5.02	4.66	1.47	2.31	2.17×10
S	683.76	6.84	2.57	9.78	5.38	1.50	2.25	4.34×10

To realize fully inelastic collisions the coefficients of restitution, static friction and dynamic friction are set to 1.0, 0.0 and 0.0. The calculation of collisions statistics is started when the particles are in equilibrium with the turbulent fluid flow. Figure 6 illustrates a typical snapshot of a cutting plane with particles suspended in the turbulent fluid flow. In addition, Table 2 gives an overview of several nondimensional particle properties and collision statistics which were averaged over the last ten eddy turnover times. In the following, the Kolmogorov scales are used to normalize the specific particle properties and collision statistics such as the collision time τ_C, since the particle diameter is smaller than the smallest turbulent length scales.

The reference volume fraction of the dispersed phase α_P is set to 0.001, so that the given system is within the dilute limit, with regard to Elghobashi [43]. Moreover, as shown in Table 2 Case A-F, the mass loading m_P/m_F is sufficiently small to neglect the influence of the particle phase on the fluid flow, also known as one-way coupling. But as the effect of α_P especially for higher collision frequencies is of interest, the volumetric fraction of the dispersed phase is stepwise increased to 0.005 (Case G-M) and 0.01 (Case N-S). In order to achieve results, which are methodological comparable to the results obtained by the reference volume fraction $\alpha_P = 0.001$ as well as to previous studies (cf., Sundaram and Collins [12] and Fede and Simonin [15]), the assumption of one-way coupling is consistently maintained.

However, this simplification is partly affected by errors, since for larger density ratios the application of two-way coupling (i.e., turbulence modulation by the particles) may be more appropriate, e.g., Case L-M and Q-S. Nevertheless, the resulting enlarged mass loadings coincide with those used in Ref. [12]. Finally, the probable position of two colliding particles is not influenced by their finite size (i.e., no close-packing effect), since the volume fraction is less than 0.05 [15].

3.4 Free Path Between Particle Collisions. Nevertheless, the used solid volume fractions are small enough to ensure that the mean free path of particles is of the order of the Kolmogorov length scale. Here, the free path is defined as a traveled distance of a single particle between two subsequent inter-particle collisions. Figure 10 shows exemplarily the probability density function of the free path of particles as a function of three different particles Stokes numbers *St*. In the present work, *St* characterizes the particle response behavior regarding to the smallest turbulent

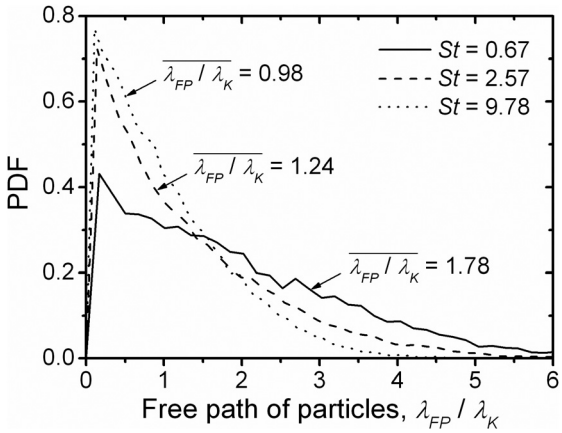

Fig. 10 Probability density function of the free path between particle collisions depending on the particle Stokes number *St* ($\alpha_P = 0.01$). The indicated particle mean free path $\overline{\lambda_{FP}}$ is also normalized by the Kolmogorov length scale λ_K.

structures and is defined as ratio of particle response time to Kolmogorov timescale $St = \tau_P/\tau_K$. The resulting Stokes numbers are between 0.34 and 9.79 (see Table 2).

According to Fig. 10, the global maxima of the PDFs are generally in the range of the particle radius or rather a quarter of the Kolmogorov length scale. However, the width of the distributions is shifted with increasing Stokes number towards smaller values. This qualitative impression may be underlined by the mean free path $\overline{\lambda_{FP}/\lambda_K}$ which was averaged over all tracked particles and normalized by the Kolmogorov length scale. Hence, particles with Stokes numbers smaller than unity mostly collide with neighboring particles after at least one turnover of a Kolmogorov eddy, whereas particles with larger Stokes numbers collide shortly before a rotation of such an eddy is finished. Moreover, the present mean free paths illustrate that even for the largest used volume fraction collisions of particles are based on small scale phenomena and are not affected by the applied artificial forcing scheme.

3.5 Analysis of Solid Volume Fraction Effects. In this study, the probability of inter-particle collisions mainly depends on the fluctuating motion of the particles, the volume fraction of the dispersed phase and the inertia of solid particles, defined by particle diameter and material density. The following subsections characterize the influence of various volume fractions on the mean time between successive particle interactions. In this framework, the fluctuating particle velocity as well as the relative velocity of colliding particles and their importance to the collision behavior is also analyzed. Again, it should be pointed out that short-range phenomena such as hydrodynamic interaction of neighboring particles and the effect of fluid shortly before a collision (referred to as lubrication force) are not considered in this study.

3.5.1 Inter-Particle Collision Time. At first, the influence of various particle densities on the mean time between collisions τ_C is investigated. Here, the particle density is represented by the particle response time τ_P and; thus, by the particle Stokes number too. As shown in Fig. 11, the time between two successive inter-particle collisions is continuously decreased with increasing Stokes number. Moreover, the collision time seems to converge asymptotically to a finite value when the inertia of particles is becoming more and more important. In more general terms, the computed collision times are decreasing with increasing volume fraction while retaining a constant Stokes number. This trend is valid along the varied range of Stokes numbers. The resulting offset between the different α_P will be analyzed in more detail by

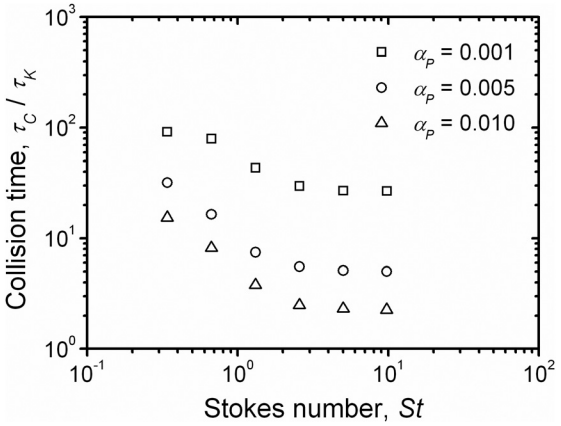

Fig. 11 Effect of the particle response behavior (i.e., *St*) on the mean time between two particle-particle collisions τ_C: Here, the particle response time τ_P is normalized by the constant Kolmogorov timescale τ_K and plotted against the Stokes number *St* with the solid volume fraction α_P as a parameter.

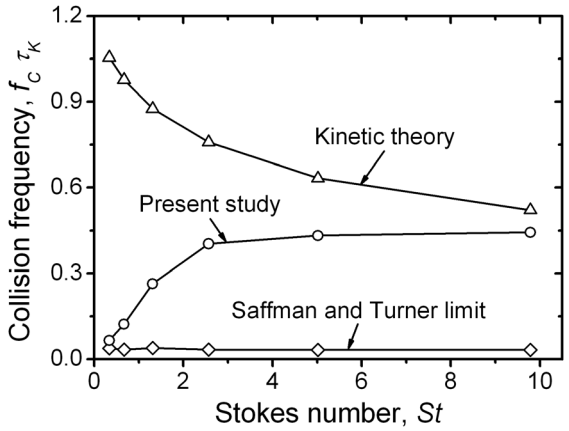

Fig. 13 Computed collision frequencies f_C as a function of the Stokes number *St* ($\alpha_P = 0.01$): Comparison of results obtained by direct numerical simulations (present study) with the analytical Saffman and Turner limit [2] as well as the kinetic theory limit [3].

means of Fig. 12. A summary of all computed collision times is given in Table 2 as well.

At this point, the particle collision frequency f_C is introduced. It is equal to the reciprocal of the collision time. For further considerations, the collision frequency is normalized by the particle response time. In Fig. 12, the resulting timescale ratios τ_P/τ_C are plotted against their corresponding Stokes numbers. As a result, the collision frequency is increased with increasing Stokes number and volume fraction as well. It may be also interesting that the obtained collision frequencies constitute, at same volume fraction, a nearly linear slope into the presented double logarithmic plot. Furthermore, the resulting straight lines may differ from each other by their scalable offset only. In accordance to Sundaram and Collins [12], squared law dependence between the analyzed volume fractions can be observed, even for Stokes numbers smaller and larger than unity.

In summary, it becomes apparent that the fluid dynamic transport of the particles is the dominant transport effect, since the time between inter-particle collisions is larger than the particle response time (see Ref. [22] for more cases). The particle motion may be mainly governed by small scale fluid phenomena such as shear and acceleration mechanism. Only for the Cases M, R and S, the mean collision time is smaller than the particle response time, whereby the particles are not able to completely respond to the fluid flow between successive collisions (see Fig. 12). Due to high collision frequencies, their motion is dominantly influenced by inter-particle collisions. Here, effects by fluid dynamic transport are of minor importance.

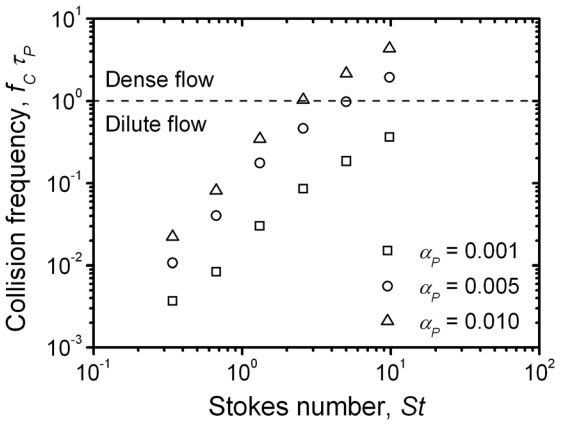

Fig. 12 Averaged collision frequencies f_C, which are normalized by their corresponding particle response times τ_P, as a function of the Stokes number *St* and solid volume fraction α_P.

According to Crowe [44], two regimes may be identified. For timescale ratios τ_P/τ_C smaller than unity, the transport of particles is based on the kinetic regime, called dilute two-phase flow. This is basically valid for most of the analyzed cases in Fig. 12. However, only for the largest analyzed Stokes numbers and volume fractions a collisional dominated regime is rudimentary reached, referred as dense two-phase flow.

3.5.2 Evaluation of Collision Frequencies. Based on the Stokes number, two limiting cases for the collision rate due to turbulence may be identified. For particles which are small compared to the Kolmogorov length scale and completely follow the turbulence, Saffman and Turner [2] provided an approximation for the collision rate due to isotopic turbulent shear, cf. Eq. (1). In this case, the Stokes number tends to zero. As previously mentioned, the other limiting case was studied by Abrahamson [3]. He analyzed the motion of heavy particles suspended in high intensity turbulence neglecting external forces, cf. Eq. (2). According to kinetic theory, particle motion is completely uncorrelated with the fluid motion. Here, the Stokes number tends to infinity. In order to be able to evaluate the collision rates determined by the DNS, the present results are compared with these two limiting cases. In this frame, the collision rates given in Eqs. (1) and (2) are simplified through the collision frequency. This is done by multiplying the obtained collision rates with the volume of the turbulent flow field. Since the particles may partially respond to turbulence, the measured collision frequencies should lie between the two analytical theories.

As shown in Fig. 13, the simulated collision frequencies begin near the Saffman and Turner limit, then rapidly increase with the Stokes number and for the larger Stokes numbers approaches the kinetic theory limit. According to the particular model limitations given in the introduction, the collision frequency given by the Saffman and Turner limit is almost solely controlled by the timescale of the smallest turbulent eddies. A similar behavior can be obtained from the present study, since for the smallest Stokes numbers the time between two successive particle-particle collisions is basically caused by fluid structures in the range of the Kolmogorov scale. On the other hand, the kinetic theory leads to a collision frequency which is mainly based on the particle velocity. This limit is nearly reached in the simulations, since with increasing particle inertia the particles become progressively less responsive to the turbulent velocity fluctuations; for example, at $St = 9.78$ (see Fig. 13).

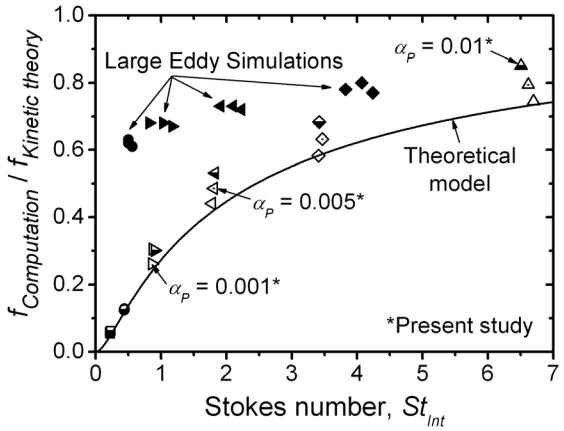

Fig. 14 Ratio of the computed collision frequency to the collision frequency obtained from kinetic theory plotted against the Stokes number St_{Int} which is based on the fluid Lagrangian integral timescale: Comparison of results obtained by direct numerical simulations (open and partly filled symbols: present study), large eddy simulations for different volume fractions (closed symbols: Laviéville et al. [21]) and analytical approximations (solid line: Kruis and Kusters [5]). Note: Symbols of one shape represent a comparable Stokes number, e.g., circle, square or triangle. Moreover, symbols of one filling level (present DNS) indicate the results for different volume fractions, i.e., ◁:$\alpha_P = 0.001$, ◁:$\alpha_P = 0.005$, ◀:$\alpha_P = 0.01$.

An additional comparison with other analytical and numerically evaluated turbulent collision frequencies is presented in Figure 14. Here, the computed collision frequencies are normalized by their corresponding collision frequencies obtained from the kinetic theory limit, which is more probable in numerous industrial two-phase flows than the Saffman and Turner limit. Since Laviéville et al. [21] did not specify values for the Kolmogorov timescale in their large eddy simulations (LES), which are used for comparison among others, the presented Stokes numbers are based in Fig. 14 on the ratio of particle response time τ_P to fluid Lagrangian integral timescale $\tau_{L,F}$, given in Table 2 as well. Figure 14 demonstrates that in the present DNS for small Stokes numbers the variation of volume fraction has no considerable effect on the rate at which particles collide. As discussed above, the motion of light particles is almost controlled by the small scale velocity fluctuations. For this reason, collisions between particles have no remarkable influence, since the post-collision velocities immediately retrieve their underlying fluid streamlines. Hence, different volume fractions are insignificant with regard to the achieved collision frequencies.

But as shown in Figure 14, the influence of the volume fraction on the collision frequency increases rapidly with increasing Stokes number. Moreover, the collision frequencies themselves approach successively the upper limiting value of unity, which stands for an ideal realization of the kinetic theory and; thus, a completely random particle motion. It should be pointed out that with increasing particle inertia the corresponding centrifugal forces, which act on the particles, are increasing as well. Therefore, the particle velocities become more and more uncorrelated to the fluid velocities viewed by the particles. The observed differences between the investigated volume fractions are discussed in more detail within the next subsections. Nevertheless, the collision frequency is basically increased with increasing volume fraction, while retaining an almost constant Stokes number.

Furthermore, previously performed large eddy simulations, published by Laviéville et al. [21], are consulted for an additional comparison. It must be mentioned that a concrete differentiation between the various volume fractions obtained from the LES is unfortunately not possible with the data available in the paper [21]. Notwithstanding, large differences between the DNS and LES can be observed in the range of small Stokes numbers (see Figure 14). On the other hand, the DNS and LES tend to approach each other for larger Stokes numbers. This rapprochement can be explained by the fact that heavy particles partly respond to small scale velocity fluctuations only. As a result, the motion of inertial particles is less dependent by the smallest turbulent eddies. Besides, it is well known that in large eddy simulations the large scales of the turbulent fluid flow are directly resolved, whereas the sub-grid fluid turbulence effects are described either by a functional or by a structural model. Therefore, the collision frequency of heavier particles is more similar between LES and DNS results, cf. diamonds at $St_{Int} \approx 4.0$ in Figure 14.

In contrast, the main reason for the observable discrepancy between LES and DNS at lower Stokes numbers is founded in the modeling of the fluid field, since in the LES the effect of sub-grid turbulence on the particle motion is not accounted for [21]. At this point, investigations by Fede and Simonin [15] are used for further considerations. In that study, effects of sub-grid fluid turbulence on the motion of nonsettling colliding particles suspended in steady homogeneous isotropic turbulent flow were analyzed by a successive low-passed flow field. They demonstrated that for particles with small Stokes numbers the sub-grid fluid velocity fluctuations are perceptible as a random force. According to Ref. [15], the calculation of the motion of point-particles should be supplemented by a Langevin or eddy-lifetime model. Regrettably, none of those models were applied or mentioned in the article about the given LES [21].

In addition, Fede and Simonin [15] suggested that in case of very small Stokes numbers a complex interaction between particles and the smallest turbulent eddy structures occurs. However, the relevant sub-grid fluid velocity gradients are unknown in LES [15]. In conclusion, it can be pointed out that the LES is only partly suitable for investigations of phenomena driven by particle interaction with small-scale turbulence structures, especially for small Stokes numbers. Hence, the differences between LES and DNS with decreasing Stokes number become more apparent (see Fig. 14).

Another analytical expression for the collision rate was proposed by Kruis and Kusters [5]. Following their conclusions [5], the acceleration mechanism is only considered for the expression of the relative particle velocity, whereas the contribution due to viscous shear is neglected. Moreover, the Cunningham slip factor is set to unity, since the particle size is far beyond the Brownian regime. In addition, the influence of the particle phase on the fluid flow is neglected as well as inter-particle collisions. More limitations were not provided for the universal solution given in Eq. (3). In conclusion, the developed approximation mainly depends on the relative velocity of particle pairs as well as on large scale fluid properties such as the turbulent velocity fluctuations u', the integral timescale τ_{Int} and the turbulent dissipation rate ε.

Both the results obtained from theoretical approximation and direct numerical simulations follow the same trend about the whole range of Stokes numbers. The theory [5] agrees very well with the LBM simulations for the smallest volume fraction of solids over the entire range of Stokes numbers. This is expected, since the theory neglects inter-particle collisions and their importance in the DNS is still not very large. With increasing particle volume fraction in the DNS, the collision frequency is decisively rising for $St_{Int} > 1$. In the case of $St_{Int} < 1$, there is almost no effect as discussed above.

3.5.3 Fluctuating Particle Motion. This subsection analyzes the effect of the solid volume fraction on the particle fluctuating motion which may be characterized by the Lagrangian integral timescale. This timescale can be integrated along the particle trajectories using the following Lagrangian correlation function $R_{P,u}(\tau)$ which is based on the recorded particle velocities:

$$R_{P,u}(t + i\Delta t) = \frac{1}{N_k} \sum_{i}^{k} \frac{\mathbf{u_P}(t_0) \cdot \mathbf{u_P}(t + i\Delta t)}{\sqrt{\overline{\mathbf{u_P}^2(t_0)} \cdot \overline{\mathbf{u_P}^2(t + i\Delta t)}}} \tag{49}$$

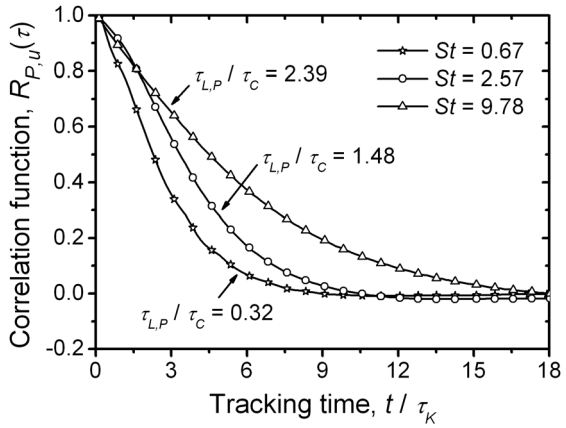

Fig. 15 Averaged Lagrangian correlation functions of the particle velocities $R_{P,u}(\tau)$ and their corresponding Lagrangian integral timescales $\tau_{L,P}$ as a function of the particle Stokes number St ($\alpha_P = 0.01$).

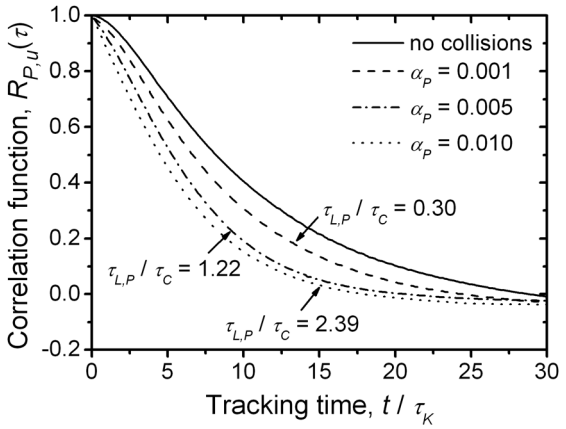

Fig. 16 Influence of the volume fraction α_P on the Lagrangian correlation functions of the particles $R_{P,u}(\tau)$ in presence as well as in absence of inter-particle collisions ($St = 9.78$). In case of particle-particle collision, the ratio of the particle Lagrangian integral timescale to the mean time between two successive inter-particle collisions $\tau_{L,P}/\tau_C$ is given as well.

where N_k is the total number of particle samples. In order to improve the fundamental understanding, different $R_{P,u}(\tau)$ are firstly compared on the basis of the particle inertia (see Fig. 15). The curve progression shifts with increasing Stokes number towards larger correlation coefficients. Since inertial particles are less responsive with respect to turbulence, their velocity changes to a large extent by inter-particle collisions which are more frequent than for small particle Stokes numbers (see Fig. 12). As a consequence, between successive particle collisions their velocity is hardly changing. Particles with small Stokes numbers experience less collisions and acquire more easily fluid fluctuations between collisions through the smallest turbulent eddies. This implies that the velocity of particles with large Stokes numbers is more correlated than that of particles with small St (see Fig. 15).

This effect can be also identified from the ratio of the particle Lagrangian integral timescale $\tau_{L,P}$ to the mean time between two successive inter-particle collisions τ_C, which is also shown in Fig. 15. Unfortunately, the exact transition point between a particle motion uncorrelated by the induced fluid dynamic transport and the prevailing occurrence of inter-particle collisions could not be resolved with the data available. In summary, the computed particle Lagrangian integral timescales are also summarized in Table 2.

Moreover, the volume fraction as well as the absence or presence of inter-particle collisions has a visible influence on the shape of the particle Lagrangian correlation functions (see Sommerfeld [22]). As shown in Fig. 16, the absence of particle-particle collisions leads to higher correlation coefficients, since the particle motion is solely affected by the turbulent flow field. In consideration of inter-particle collisions, the shape of the correlation functions is shifted with increasing volume fraction towards smaller correlation coefficients. With increasing volume fraction the trajectories of particles are increasingly deflected through the occurrence of particle-particle collisions, leading to a more uncorrelated motion of the particles, i.e., decrease of $\tau_{L,P}$. On the other hand, the collision time is reduced at a faster rate with increasing volume fraction yielding a remarkable decrease of the timescale ratio $\tau_{L,P}/\tau_C$ (see Fig. 11).

For the smallest volume fraction, the particle Lagrangian integral timescale is smaller than the mean time between two successive inter-particle collisions. Based on $\alpha_P = 0.001$, the particle transport is mainly affected by the motion through the unsteady eddies yielding $\tau_{L,P}/\tau_C = 0.30$. As already mentioned, for larger volume fractions the probability of particle-particle collision is much higher (Fig. 11). As a consequence, the ratio $\tau_{L,P}/\tau_C$ is noticeable increased towards larger values with increasing volume fraction (see Fig. 16). In case of the largest volume fraction $\alpha_P = 0.01$, the particle Lagrangian integral timescale is more than two times larger than the mean collision time. It becomes apparent that the particle motion is more pronounced affected by inter-particle collisions, i.e., decorrelation of particle velocities.

In order to manifest the relative importance of turbulence and collision induced particle transport as well as particle inertia (i.e., St), the timescale of particle velocity change $\tau_{L,P}$ may be compared with the Kolmogorov and the inter-particle collision timescale and plotted versus the Stokes number with the particle volume fraction as a parameter (Fig. 17). A general trend of the change of both timescale ratios with regard to rising Stokes numbers is a continuous increase. This is associated with an increase of the particle Lagrangian integral timescale $\tau_{L,P}$ as particle inertia increases and their motion is less influenced by turbulence, i.e., particles move on more or less straight paths between successive collisions (see Fig. 15). This comprises that the particle motion becomes more correlated. Although $\tau_{L,P}$ is becoming larger with the Stokes number, the timescale ratio $\tau_{L,P}/\tau_C$ is also increasing as the collision timescale is reduced at a faster rate (see Fig. 11).

Naturally, the collision rate between particles is increasing (i.e., decreasing τ_C) with increasing particle volume fraction. As an outcome, the timescale ratio $\tau_{L,P}/\tau_C$ is also rising, more

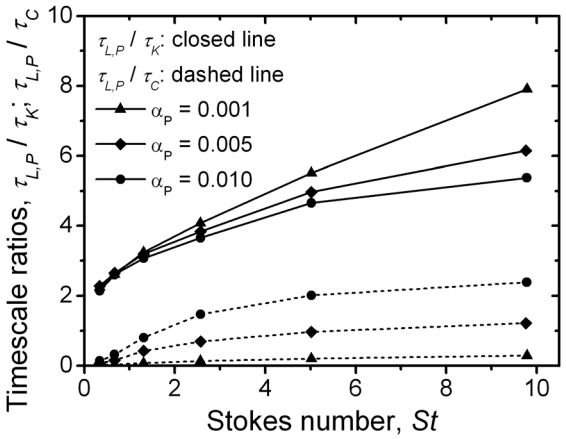

Fig. 17 Particle Lagrangian integral timescales $\tau_{L,P}$ as function of the Stokes number St with the solid volume fraction α_P as a parameter: The calculated timescales are normalized by the Kolmogorov timescale τ_K as well as the mean time between successive inter-particle collisions τ_C.

pronounced, however, for particles with Stokes numbers larger than unity. For small particle Stokes numbers, this timescale ratio does not change very much as they easily follow turbulence, whereby the collision rate does not vary significantly with volume fraction (Fig. 17). Also the timescale ratio $\tau_{L,P}/\tau_K$ is not very much dependent on particle volume fraction for Stokes numbers below about 1.5 implying that the Lagrangian particle velocity correlation function should be almost identical. For larger Stokes numbers, however, the timescale ratio $\tau_{L,P}/\tau_K$ is remarkably decreased with increasing particle volume fraction. This means that the particle motion becomes more and more decorrelated as a consequence of the increasing collision rate and the resulting faster change of particle velocity (Figs. 16 and 17). As a result, the values of $\tau_{L,P}/\tau_K$ and $\tau_{L,P}/\tau_C$ are shifted towards each other with increasing volume fraction (i.e., $\tau_{L,P}/\tau_K$ decreases and $\tau_{L,P}/\tau_C$ increases) indicating the growing importance of inter-particle collisions. For all considered cases, the values of $\tau_{L,P}/\tau_K$ are much larger than those for $\tau_{L,P}/\tau_C$. This indicates that the particle velocity change is primarily affected by the competition between turbulence and particle inertia.

As already indicated above, the occurrence of inter-particle collisions has only a minor effect on the mean kinetic energy of the particles. In support of this statement, the ratio of the kinetic energy of the particle fluctuating motion k_P to the turbulent kinetic energy of the flow field k_F as a function of the particle Stokes number is given in Fig. 18. In compliance with other DNS such as Ref. [15], k_F was extracted at the particle position, whereby the inter-phase transfer of turbulent kinetic energy and; thus, the dissipation at the particle surface might not be correctly captured. Nevertheless, k_P decreases continuously, since the particles become less responsive to the turbulent fluctuations with increasing Stokes number. Furthermore, different volume fractions have no considerable influence on the measured kinetic energy of the particles. This is expected, since the energy in the system should be conserved when treating inter-particle collisions as ideal (i.e., $e=1$ and $\mu=0$).

Besides, the present ratio k_P/k_F is also compared with results from other DNS, published by Sundaram and Collins [12] and Fede and Simonin [15]. As a result, the computed ratios of the kinetic energy show a quantitative good agreement with the results available in the literature. The visible offset between the plotted values may be identified by their different Taylor Reynolds numbers Re_T applied in the simulations. In this connection, a larger Re_T represents for instance a higher energy content of the turbulent fluid structures. Hence, the kinetic energy ratios of the present DNS are shifted towards smaller values.

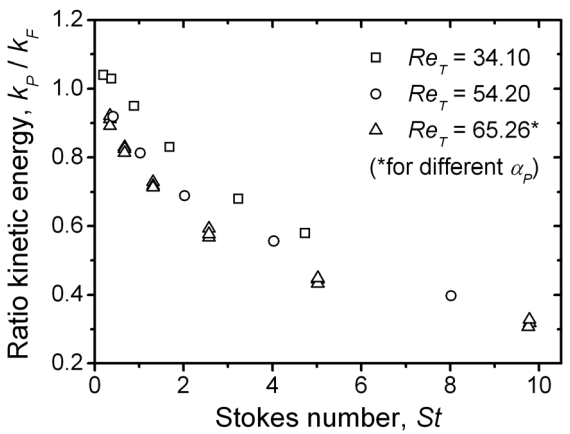

Fig. 18 Comparison of the ratio of kinetic energy of the particle fluctuation motion k_P to the turbulent kinetic energy of the flow field k_F obtained by the present DNS (triangle: $Re_T = 65.26$) with results from other DNS, published by Sundaram and Collins [12] (circle: $Re_T = 54.20$) and Fede and Simonin [15] (square: $Re_T = 34.10$), depending on the Stokes number St (Note: (1) symbols of one kind indicate the results for the different volume fractions, and (2) the results of all three DNS are based on a one-way momentum coupling of the dispersed phase with the fluid flow).

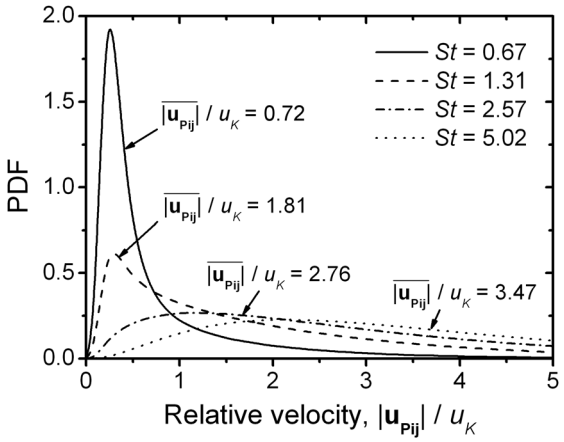

Fig. 19 Probability density function of the relative velocity modulus of colliding particles $|\mathbf{u}_{Pij}|$ which is normalized by Kolmogorov velocity u_K with the Stokes number St as a parameter ($\alpha_P = 0.01$). In addition, the mean values of relative velocity modulus are printed for easy comparison.

3.5.4 Relative Velocity of Colliding Particles. The last subsection describes the influence of the solid volume fraction on the relative motion between colliding particles. To get a basic idea about the initial relative motion during the approach of particles, the probability density functions of the relative velocity modulus $|\mathbf{u}_{Pij}|$ between colliding particles at constant volume fraction are firstly analyzed. According to the previously discussed results, it is not surprising that the velocities of light colliding particles are strongly correlated. Hence, the relative velocity modulus $|\mathbf{u}_{Pij}|$ is generally of the order of the smallest eddy-turnover velocities, also known as Kolmogorov velocity u_K (see Fig. 19). For such Stokes number particles, the probability of small relative velocities is increased, because fluid and particle velocities tend to be aligned. In this regime, the correlation between fluid and particle velocities is more pronounced as the probability of correlated velocity modulus between approaching particles, since the mean $|\mathbf{u}_{Pij}|$ is smaller than u_K.

Due to the increasing inertia of heavier particles, this behavior is less distinct. For this reason, the maximum of the PDFs is shifted towards larger relative velocities as well as the width of the distributions increase. As a consequence, the mean relative velocity of colliding particles exceeds the magnitude of the Kolmogorov velocity (Fig. 19). Hence, possible collision partners may also originate from different neighboring eddy structures. Moreover, large Stokes number particles may travel largely on almost straight paths from different regions.

In Fig. 20, the mean relative velocity and the associated mean angle upon particle collision are shown in dependence of the Stokes number with the particle volume fraction as a parameter. Here, the particle velocity angle φ at the time of collision is defined as:

$$\varphi = \arccos\left(\frac{\mathbf{u}_{Pi} \cdot \mathbf{u}_{Pj}}{|\mathbf{u}_{Pi}| \cdot |\mathbf{u}_{Pj}|}\right) \tag{50}$$

As shown in Fig. 20, the obtained mean relative velocity and the mean velocity angle at the instant of collision show the same trends with regard to Stokes number and particle volume fraction. With increasing Stokes number, both values (i.e., $\overline{|\mathbf{u}_{Pij}|}/u_K$ and $\overline{\varphi}$) are rapidly increasing approaching a limiting value. This is

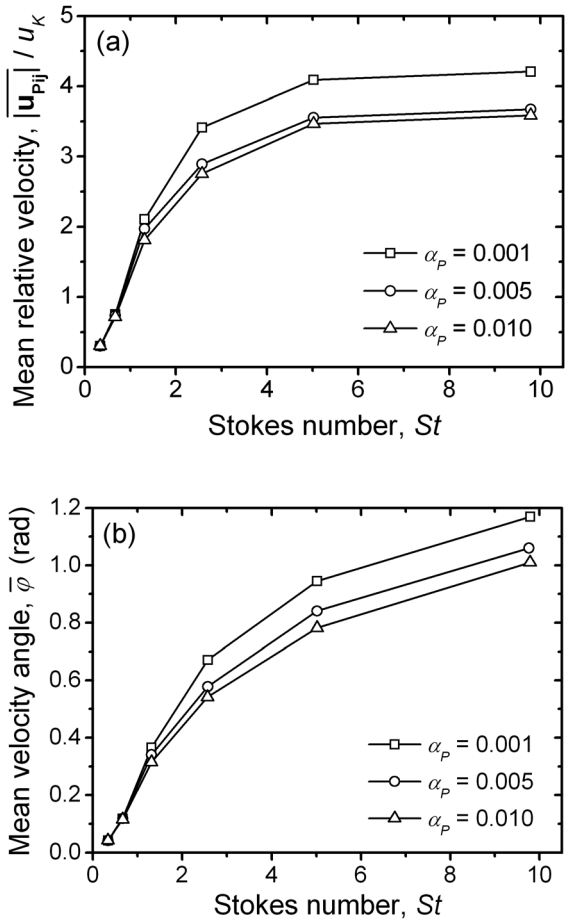

Fig. 20 Influence of the volume fraction α_P on (*a*) the mean relative velocity modulus $\overline{|\mathbf{u}_{Pij}|}$ and (*b*) the mean particle velocity angles $\bar{\varphi}$ between colliding particles as a function of the Stokes number *St*.

basically the result of growing randomness of colliding particle trajectories, i.e., inertial colliding particles may come on rather straight trajectories from completely different directions as they are less responsive to turbulence and achieved a deflection from previous collisions.

The motion of particles with small Stokes number is strongly correlated with the fluid, whereby colliding particles move almost with the same velocity and their collision angle is very small, i.e., the particles have very similar trajectories as they are moving in the same eddy. Hence, different volume fractions and, thereby, inter-particle collisions have no remarkable influence on the motion of very light particles, since the particle motion is mainly dominated through the transport induced by turbulent velocity fluctuations (see also Fig. 17).

Besides, Fig. 20 demonstrates that the effect of volume fraction becomes more and more important with increasing particle inertia, particularly for Stokes numbers larger than unity. At larger α_P, the probability of a particle collision is certainly increased (see Fig. 11). The reduction of the particle relative velocity and collision angle with increasing particle volume fraction, especially at higher Stokes numbers, may be substantiated by the following arguments.

At low volume fraction, highly inertial particles are almost homogeneously distributed in the flow field and will be transported by all turbulent structures, at least partly, i.e., there is almost no preferential concentration [45]. This yields in average larger values of the collision velocity and angle.

With increasing volume fraction, the collision rate is enhanced yielding a clustering of the particles. This is originated in the fact that particles are being trapped in such clusters due to inter-particle collisions, i.e., particles intending to move out of the cluster are bounced back due to collisions with particles coming from outside the cluster. Adopting the concept of preferential concentration, these clusters are formed in regions of low vorticity and high strain rate. As the particle residence time in these clusters is larger compared to the other regions, the particles have more time to align their motion with the flow field, apart from some collision effects. This will result ultimately in reduced average particle relative velocities and collision angles (Fig. 20). However, this idea will need further investigations.

4 Conclusions

Direct numerical simulations of particle-laden homogeneous isotropic turbulence were performed to characterize the collision behavior for different particle Stokes numbers and volume fractions. The fluid motion was computed using a three-dimensional Lattice-Boltzmann method including a spectral forcing scheme to generate the unsteady turbulence field. Under assumption of point-particles, the transport of mono-disperse spherical particles was modeled in a Lagrangian frame of reference. Since in the selected gas-particle system the ratio of particle material density to fluid density was sufficient large, the drag force is dominating the particle motion [33]. Hence, this force was considered in the equation of motion only. The modeling of collisions between solid particles was based on a deterministic collision model. According to other DNS [12,15], the influence of the particle phase on the fluid flow was neglected. Moreover, short-range phenomena such as hydrodynamic interaction of neighboring particles and the presence of fluid shortly before a collision were also not considered, which should be kept in mind.

As the deterministic inter-particle collision model was newly implemented in the in-house LBM code, it was first validated for a fluid-free granular medium yielding a very good agreement with kinetic theory.

The main emphasis of the present contribution was, however, directed towards the analysis of the influence of particle volume fraction α_P and; hence, inter-particle collisions on the transport of nonsettling inertial particles in homogeneous isotropic turbulence. In all the simulations, the particle diameter was kept constant at a value of 0.58 times the Kolmogorov length scale, and the variation of particle Stokes number St (i.e., in the range of 0.34 to 9.79) was achieved by adapting the particle material density. The particle response behavior was characterized by a statistical evaluation of the simulation data with respect to collision mean free paths, inter-particle collision times and frequencies, Lagrangian correlation functions of particle velocities, including resulting integral timescales, as well as collision angles and relative velocities. For most of the cases considered, the particle transport was dominantly affected by the smallest scales of turbulence implying that the particle response time was smaller than the mean inter-particle collision time, except for a few cases with the higher Stokes number and particle volume fraction.

The increase of the Stokes number for given particle volume fractions showed that the simulations correctly predict the increase of the collision frequency from the Saffman and Turner limit (particles completely follow turbulence: $St \rightarrow 0$) to the kinetic theory limit (random particle motion $St \rightarrow \infty$). Moreover, the predicted collision frequencies as a function of Stokes number are in close agreement to the theory of Kruis and Kusters [5] for the lowest particle volume fraction considered. Increasing particle concentration yields growing collision frequencies, but only for $St \geq 1$. For smaller Stokes numbers, volume fraction has almost no effect. It could be shown that LES does not properly predict collision statistics, if sub-grid particle transport is neglected.

The analysis of the Lagrangian correlation function of particle velocities with regard to particle inertia (i.e., St) and particle volume fraction allows further important conclusions regarding the effects governing particle behavior. In summary, this can be also

done by considering the timescale of particle velocity change $\tau_{L,P}$ (i.e., particle Lagrangian integral timescale) with respect to the Kolmogorov timescale and the inter-particle collision time. This analysis allows for following conclusions:

- Increasing particle Stokes number for a given volume fraction results in a more correlated particle motion as particle paths between subsequent collisions become noticeably more straight, i.e., heavier particles are less affected by turbulence.
- Hence, with increasing Stokes number $\tau_{L,P}$ is also increasing, i.e., particle motion becomes more correlated.
- Increasing particle volume fraction decorrelates particle motion perceptibly for larger Stokes numbers due to rising collision frequency.
- The motion of light particles (i.e., $St < 1$) is hardly affected by particle volume fraction, i.e., the timescale of particle velocity change $\tau_{L,P}$ is almost constant for given Stokes numbers.

Finally, also the relative motion of particles upon collision was analyzed. As expected, the velocity of colliding particles is strongly correlated for small Stokes numbers and becomes increasingly uncorrelated with rising Stokes number. The mean relative velocity and velocity angle of colliding particles in dependence of the Stokes number showed a pronounced effect of α_P, again only for $St > 1$. The reduction of the relative velocity and the velocity angle with growing volume fractions may be explained by particle clustering occurring as a result of inter-particle collisions, which was observed in the present simulation results. Within a cluster, particles reside relatively long and have a more or less mutual behavior. As a consequence, the mean collision velocity and angle are reduced with rising volume fraction.

For clarification, however, a further characterization of particle clustering effects in dependence of particle volume fraction is envisaged. In addition, the effect of finite particle size (i.e., resolved particles) will be considered, allowing also accounting for fluid-dynamic interactions of colliding particles.

Acknowledgment

The financial support of the present studies by the Deutsche Forschungsgemeinschaft under Grant No. SO 204/33-1,2 is gratefully acknowledged. Furthermore, the authors would like to thank Dipl.-Ing. M. Dietzel for his support and many helpful discussions.

Nomenclature

Latin Symbols

$\mathbf{a}$ = acceleration of fluid velocity
$\mathbf{a_F}$ = forcing acceleration
C = universal Kolmogorov constant
c = grid constant
c_d = drag coefficient
c_s = speed of sound
DNS = direct numerical simulation
d_P = particle diameter
E = three-dimensional energy spectrum
E_x = one-dimensional transverse energy spectrum
$\mathbf{e}$ = coefficient of restitution
$\mathbf{e_n}$ = normal unity vector
$\mathbf{e_t}$ = tangential unity vector
$\mathbf{F_d}$ = drag force
F_{ext} = external force
$\mathbf{F_i}$ = different relevant forces
f_C = collision frequency
$f_{\sigma i}$ = discrete distribution function
$f_{\sigma i}^{(0)}$ = discrete equilibrium distribution function
$\mathbf{J}$ = momentum
$\mathbf{k}$ = wave number
k_F = turbulent fluid kinetic energy
k_P = kinetic energy of particle motion
LBM = Lattice-Boltzmann method
L_{Box} = length of domain in one direction
LES = large eddy simulation
m_F = fluid mass
m_P = particle mass
m_{Peff} = effective particle mass
N = collision rate per unit volume and time interval
N_{Cells} = number of cells
N_k = number of samples
n_P = particle number concentration
PDF = probability density function
p = pressure
$R_{P,u}(\tau)$ = correlation function of particle velocity
Re_P = particle Reynolds number
Re_T = taylor Reynolds number
r.m.s. = root mean square
St = particle Stokes number
T_F = correlation timescale
t = time
$\mathbf{u}$ = fluid velocity
u' = root mean square of fluid velocity fluctuations
u_K = Kolmogorov velocity
$\mathbf{u_P}$ = particle velocity
$\mathbf{u_{Pij}}$ = relative particle velocity
$\mathbf{u_{Pij,t}}$ = tangential component of relative particle velocity at the point of contact
$\mathbf{u_P^*}$ = post-collision particle velocity
$\mathbf{u_{Pij}^*}$ = post-collision relative particle velocity
$\mathbf{x}$ = fluid position
$\mathbf{x_P}$ = particle position
$\mathbf{x_{Pij}}$ = relative particle position
Z_F = forcing cut-off function

Greek Symbols

α_P = volume fraction of particle phase
Γ = Gaussian random number
Δt = time step of fluid phase
$\Delta t_{ij,c}$ = collision time for overlapping particles
Δt_P = particle time step
Δx = spatial discretization
ε = dissipation rate
ζ = abruptness of cut-off
η = dynamic fluid viscosity
λ_{FP} = free path between two inter-particle collisions
λ_{Int} = integral length scale
λ_K = Kolmogorov length scale
λ_T = Taylor length scale
μ_d = dynamic coefficient of friction
μ_s = static coefficient of friction
ν = kinematic fluid viscosity
$\boldsymbol{\xi_{\sigma i}}$ = discrete velocity of fluid elements
ρ = fluid density
ρ_P = particle material density
σ_F = forcing amplitude
τ = relaxation parameter
τ_C = time between two inter-particle collisions
τ_{Int} = integral timescale
τ_K = Kolmogorov timescale
$\tau_{L,F}$ = fluid Lagrangian integral timescale
$\tau_{L,P}$ = particle Lagrangian integral timescale
τ_P = particle response time
φ = particle velocity angle
ψ = skew parameter
ψ_0 = limiting skew parameter
$\omega_{\sigma i}$ = weighting factor of the discrete equilibrium function

References

[1] Ho, C. A., and Sommerfeld, M., 2002, "Modelling of Micro-Particle Agglomeration in Turbulent Flow," Chem. Sci. Eng., **57**, pp. 3073–3084.

[2] Saffman, P. G., and Turner, J. S., 1956, "On the Collision of Drops in Turbulent Clouds," J. Fluid Mech., **1**, pp. 16–30.
[3] Abrahamson, J., 1975, "Collision Rates of Small Particles in a Vigorously Turbulent Fluid," Chem. Eng. Sci., **30**, pp. 1371–1379.
[4] Williams, J. J. E., and Crane, R. I., 1983, "Particle Collision Rate in Turbulent Flow," J. Multiphase Flow, **9**, pp. 421–435.
[5] Kruis, F. E., and Kusters, K. A., 1997, "The Collision Rate of Particles in Turbulent Flow," Chem. Eng. Comm., **158**, pp. 201–230.
[6] Mei, R., and Hu, K. C., 1999, "On the Collision Rate of Small Particles in Turbulent Flows," J. Fluid Mech., **391**, pp. 67–89.
[7] Alipchenkov, V. M., and Zaichik, L. I., 2001, "Particle Collision Rate in Turbulent Flow," J. Fluid Dynamics, **36**, pp. 608–618.
[8] Wang, L. P., Ayala, O., Kasprzak, S. E., and Grabowski, W. W., 2005, "Theoretical Formulation of Collision Rate and Collision Efficiency of Hydrodynamically Interacting Cloud Droplets in Turbulent Atmosphere," J. Atmos. Sci. **62**, pp. 2433–2450.
[9] Zaichik, L. I., Alipchenkov, V. M., and Avetissian, A. R., 2006, "Modelling Turbulent Collision Rates of Inertial Particles," Int. J. Heat Fluid Flow, **27**, pp. 937–944.
[10] You, C., Zhao, H., Haiying, Y. C., Qi, H., and Xu, X., 2004, "Experimental Investigation of Interparticle Collision Rate in Particulate Flow," Int. J. Multiphase Flow, **30**, pp. 1121–1138.
[11] Salazar, J. P. L. C., De Jong, J., Cao, L. J., Woodward, S. H., Meng, H., and Collins, L. R., 2008, "Experimental and Numerical Investigation of Inertial Particle Clustering in Isotropic Turbulence," J. Fluid. Mech., **600**, pp. 245–256.
[12] Sundaram, S., and Collins, L. R., 1997, "Collision Statistics in an Isotropic Particle-Laden Turbulent Suspension. Part 1. Direct Numerical Simulations," J. Fluid Mech., **335**, pp. 75–109.
[13] Wang, L.-P., Wexler, A. S., and Zhou, Y., 1998, "On the Collision Rate of Small Particles in Isotropic Turbulence. I. Zero-Inertia Case," Phys. Fluids **10**, pp. 266–276.
[14] Février, P., Simonin, O., and, Legendre, D., 2001, "Particle Dispersion and Preferential Concentration Dependence on Turbulent Reynolds Number from Direct and Large-Eddy Simulations of Isotropic Homogeneous Turbulence," *Proceedings of 4th International Conference on Multiphase Flow*, New Orleans, Louisiana, pp. 1–12.
[15] Fede, P., and Simonin, O., 2006, "Numerical Study of the Subgrid Fluid Turbulence Effects on the Statistics of Heavy Colliding Particles," Phys. Fluids, **18**, p. 045103.
[16] Ten Cate, A., Derksen, J. J., Portela, L. M., and van den Akker, H. E. A., 2004, "Fully Resolved Dimulations of Colliding Monodisperse Spheres in Forced Isotropic Turbulence," J. Fluid Mech., **519**, pp. 233–271.
[17] Uhlmann, M., 2005, "Interface-Resolved Direct Numerical Simulations of Vertical Particulate Channel Flow in the Turbulent Regime," Phys. Fluids, **20**, p. 053305.
[18] Lucci, F., Ferrante, S., and Elghobashi, S., 2010, "Modulation of Isotropic Turbulence by Particles of Taylor Length-Scale Size," J. Fluid Mech., **650**, pp. 5–55.
[19] Dietzel, M., Ernst, M., and Sommerfeld, M., 2011, "Application of the Lattice-Boltzmann-Method in Two-Phase Flow Studies: From Point-Particles to Fully Resolved Particles," Proceedings of ASME-JSME-KSME Joint Fluid Engineering Conference 2011, Paper No. AJK2011-04033.
[20] Wang, L.-P., Rosa, B., Gao, H., He, G., and Jin, G., 2009, "Turbulent Collision of Inertial Particles: Point-Particle Based, Hybrid Simulations and Beyond," Int. J. Multiphase, **35**, pp. 854–867.
[21] Laviéville, J., Deutsch, E., and Simonin, O., 1995, "Large Eddy Simulation of Interactions Between Colliding Particles and a Homogeneous Isotropic Turbulence Field," *Gas-Solid-Flows*, **228**, pp. 347–357 .
[22] Sommerfeld, M., 2001, "Validation of a Stochastic Lagrangian Modelling Approach for Inter-Particle Collisions in Homogeneous Isotropic Turbulence," Int. J. Multiphase Flow, **27**, pp. 1829–1858.
[23] Ladd, A. J. C., 1994, "Numerical Simulations of Particulate Suspensions via a Discretized Boltzmann Equation," J. Fluid. Mech., **271**, pp. 285–309.
[24] He, X., and Luo, L.-S., 1997, "Theory of the Lattice Boltzmann Method: From the Boltzmann Equation to the Lattice Boltzmann Equation," Phys. Rev. E, **56**(6), pp. 6811–6817.
[25] Chen, S., and Doolen, G. D., 1998, "Lattice Boltzmann Method for Fluid Flows," Annu. Fluid Mech., **30**, pp. 329–364.
[26] Bhatnagar, P. L., Gross, E. P., and Krook, M., 1954, "A Model for Collision Processes in Gases. I. Small Amplitude Processes in Charged and Neutral One-Component Systems," Phys. Rev., **94**, pp. 511–525.
[27] Guo, Z., Zheng, C., and Shi, B., 2002, "Discrete Lattice Effects on the Forcing Term in the Lattice Boltzmann Method," Phys. Rev. E., **65**, p. 046308.
[28] Dietzel, M., and Sommerfeld, M., 2010, "LBM Simulations on Agglomerate Transport and Deposition," AIP Conf. Proc., **1207**, pp. 796–801.
[29] Eswaran, V., and Pope, S. B., 1988, "An Examination of Forcing in Direct Numerical Simulations of Turbulence," Comput. Fluids **16**, pp. 257–278.
[30] Renshaw, E., 1987, "The Discrete Uhlenbek-Ornstein Process," J. Appl. Probability, **24**, pp. 908–917.
[31] Overholt, M. R., and Pope, S. B., 1998, "A Deterministic Forcing Scheme for Direct Numerical Simulations of Turbulence," Comput. Fluids, **27**, pp. 11–28.
[32] Sommerfeld, M., van Wachem, B., and Oliemans, R., 2008, "Computational Fluid Dynamics of Dispersed Multi-Phase Flows," *ERCOFTAC Best Practice Guidelines, European Research Community on Flow, Turbulence and Combustion*, Lausanne, Switzerland.
[33] Hjelmfelt, A. T., and Mockros, L. F., 1966, "Motion of Discrete Particles in a Turbulent Fluid," Appl. Sci. Res., **16**, pp. 149–161.
[34] Schiller, L., and Naumann, A., 1933, "Über die Grundlegenden Berechnungen bei der Schwerkraftaufbereitung," Verl. Deu. Ing., **77**, pp. 318–320.
[35] Sommerfeld, M., 1996, "Modellierung und numerische Berechnung von partikelbeladenen turbulenten Strömungen mit Hilfe des Euler/ Lagrange-Verfahrens," *Habilitation*, Shaker Verlag, Aachen, Germany.
[36] Sundaram, S., and Collins, L. R., 1996, "Numerical Considerations in Simulating a Turbulent Suspension of Finite-Volume Particles," J. Comp. Phys., **124**, pp. 337–350.
[37] Allen, M. P., and Tildesley, D. J., 1987, *Computer Simulation of Liquids*, 1st ed., Oxford University, New York.
[38] Tanaka, T., and Tsuji, Y., 1991, "Numerical Simulation of Gas-Solid Two-Phase Flow in a Vertical Pipe: On the Effect of Inter-Particle Collisions," *Gas-Solid-Flow* **121**, pp. 123–128.
[39] Decker, S., 2005, "Zur Berechnung von Gerührten Suspensionen mit dem Euler-Lagrange-Verfahren," Ph.D. thesis, Martin-Luther-Universität Halle-Wittenberg, Halle, Germany.
[40] Kolmogorov, A. N., 1991, "The Local Structure of Turbulence in Incompressible Viscous Fluid for Very Large Reynolds Numbers," Proc. R. Soc. Lond., Ser. A **434**, pp. 9–13.
[41] Yeung, P. K., and Pope, S. B., 1989, "Lagrangian Statistics From Direct Numerical Simulations of Isotropic Turbulence," J. Fluid. Mech., **207**, pp. 531–586.
[42] Maxey, M. R., and Riley, J. J., 1983, "Equation of Motion for a Small Rigid Sphere in a Nonuniform Flow," Phys. Fluids, **26**(4), pp. 883–889.
[43] Elghobashi, S., 1994, "On Predicting Particle-Laden Turbulent Flows," Appl. Sci. Res., **52**, pp. 309–329.
[44] Crowe, C. T., 1981, "On the Relative Importance of Particle-Particle Collisions in Gas-Particle Flows," Proceedings of the Conference on Gas Borne Particles, Paper No. C78/81, pp. 135–137.
[45] Coleman, S. W., and Vassilicos, J. C., 2009, "A Unified Sweep-Stick Mechanism to Explain Particle Clustering in Two- and Three-Dimensional Homogeneous Isotropic Turbulence," Phys. Fluids **21**, p. 113301.